arXiv:1203.5392v1 [nucl-th] 24 Mar 2012

The continuum discretized coupled-channels method and its applications

Masanobu Yahiro[1], Kazuyuki Ogata[2], Takuma Matsumoto[1] and Kosho Minomo[1]

[1]*Department of Physics, Kyushu University, Fukuoka 812-8581, Japan*
[2]*Research Center of Nuclear Physics (RCNP), Osaka University, Ibaraki 567-0047, Japan*

(Received March 1, 2013)

This is a review on recent developments of the continuum discretized coupled-channels method (CDCC) and its applications to nuclear physics, cosmology and astrophysics, and nuclear engineering. The theoretical foundation of CDCC is shown, and a microscopic reaction theory for nucleus-nucleus scattering is constructed as an underlying theory of CDCC. CDCC is then extended to treat Coulomb breakup and four-body breakup. We also propose a new theory that makes CDCC applicable to inclusive reactions.

Contents

1. Introduction 2
2. Theoretical foundation of CDCC 4
  2.1. Three-body CDCC 4
  2.2. Relation between CDCC and Faddeev solutions 6
3. Microscopic reaction theory for nucleus-nucleus scattering 7
  3.1. Microscopic reaction theory 7
  3.2. Validity of the Glauber model 9
  3.3. Localization of nonlocal microscopic optical potential 10
  3.4. Application of the double-folding model to the scattering of stable nuclei 11
  3.5. Application of the double-folding model to reaction cross sections for Ne isotopes 13
4. Proposal of eikonal-CDCC (E-CDCC) as a method of treating Coulomb breakup 14
5. Proposal of four-body CDCC as a method of treating breakup of three-body projectile 20
6. Proposal of the eikonal reaction theory (ERT) that makes CDCC applicable to inclusive reactions 27
  6.1. Formulation of ERT 27
  6.2. One-neutron removal reaction of ^{31}Ne 28
  6.3. Two-neutron removal reaction of ^{6}He 29
  6.4. Comparison of ERT and the Glauber model 30
7. Applications of CDCC to scattering of unstable nuclei 30
  7.1. One-neutron removal reactions of ^{18}C and ^{19}C on proton target 31
  7.2. Study on the low-lying states in the unbound nucleus ^{13}Be 32

7.3. Elastic and breakup cross sections of ^{6}He 32
8. Applications of CDCC to reactions essential in cosmology and astrophysics 35
8.1. Determination of the astrophysical factor S_{17} for the ^{7}Be$(p,\gamma)^{8}$B reaction 35
8.2. Three-body model analysis of subbarrier α transfer reaction 36
8.3. Nonresonant triple α process at low temperatures 38
9. Applications of CDCC to nuclear engineering 40
9.1. Deuteron induced reactions on ^{6,7}Li 40
9.2. Neutron induced reactions on ^{6}Li 41
10. Summary 44

§1. Introduction

Nuclear reaction is one of fundamental reactions in Nature. Understanding of nuclear reaction is important not only in nuclear physics but also in cosmology and astrophysics. The study of nuclear reaction is necessary to understand the mechanism of nucleosynthesis in the early universe, stellar evolution, and supernova explosions, and to eventually know the origin of elements in the universe. Application of the study to nuclear engineering is another important direction. The Li(d,n) reaction, for example, is regarded as one of the most promising reactions to produce intense neutron beams at the international fusion material irradiation facility (IFMIF). The study of the Li(d,n) reaction is indispensable for the engineering design of accelerator-driven neutron sources. Theoretical calculations play an important role there, since experimental data are not available systematically.

One of the most important current subjects in nuclear physics is to elucidate unstable nuclei. This subject is interesting also from the viewpoint of the origin of elements through nucleosynthesis. Unstable nuclei are considered to have exotic properties such as the halo structure1),2),3) and the loss of magicity in the "island of inversion",4) i.e., the region of unstable nuclei from ^{30}Ne to ^{34}Mg. In the island of inversion, the first-excited states have low excitation energies and large B(E2) values.5),6),7),8),9) This indicates that the $N = 20$ neutron magic number is not valid anymore. These novel quantum properties have inspired extensive experimental and theoretical studies.

Important experimental tools of investigating properties of unstable nuclei are the interaction cross section $\sigma_{\rm I}$ and the nucleon-removal cross section σ_{-N}.1),2),3),10) The experimental exploration of halo nuclei is moving from lighter nuclei such as He and C isotopes to relatively heavier nuclei such as Ne isotopes. Very lately $\sigma_{\rm I}$ was measured by Takechi and collaborators11) for $^{28-32}$Ne located near or in the island of inversion. Furthermore, a halo structure of ^{31}Ne was reported by Nakamura and his group12) with the experiment on σ_{-N}. The ^{31}Ne nucleus resides in the island of inversion and is the heaviest halo nucleus suggested experimentally in the present stage.

The elucidation of unstable nuclei can be accomplished with high-accuracy measurements of the scattering of unstable nuclei and accurate analyses of the measurements with reliable reaction theories. The scattering of unstable nuclei have two features. First, the projectile is fragile and thereby the projectile breakup becomes important. Second, measurements of the elastic scattering are not easy because of weak intensity of the secondary beam, and consequently, there is no reliable phenomenological optical potential. It is then important to construct a microscopic reaction theory that can treat the projectile breakup and does not need phenomenological optical potentials. This construction is precisely a goal of the nuclear reaction theory.

A pioneering work on the microscopic description of nucleon-nucleus scattering was done by Watson,13) which was reformulated by Kerman, McManus, and Thaler14) as series expansion in terms of an underlying nucleon-nucleon (NN) t matrix. Another important microscopic model particularly to treat inclusive reactions is the Glauber model.15) The Glauber model is based on the eikonal and the adiabatic approximation. It is well known that the adiabatic approximation makes the breakup cross section diverge when the Coulomb breakup is included. For this reason the Glauber model has been applied mainly for lighter targets in which the role of the Coulomb interaction is negligible; see, e.g., Refs. 10),16),17),18),19),20),21). Recently, a way of making Coulomb corrections to the calculations has been proposed,22),23) which works when Coulomb breakup is not so strong.

The continuum discretized coupled-channels method (CDCC)24),25) is an accurate method of treating the projectile breakup in exclusive reactions such as elastic scattering, elastic-breakup reactions, and transfer reactions. CDCC has succeeded in reproducing experimental data on the scattering of both stable and unstable nuclei; see, e.g., Refs. 26),27),28),29),30),31),32),33),34),35),36),37),38),39),40),41),42), 43),44),45),46),47),48),49),50),51),52),53),54),55),56),57),58),59) and references therein. Another reliable method of treating the projectile breakup in exclusive reactions is the dynamical eikonal approximation (DEA).60),61) The DEA is accurate at intermediate and high incident energies where the eikonal approximation is reliable.

CDCC was first proposed as a method of treating the three-body system composed of a target and two fragments of a projectile. The original version of CDCC is called three-body CDCC. In the review articles 24) and 25) on three-body CDCC, the method treated nuclear breakup but not Coulomb breakup, and the phenomenological optical potentials were mainly used as the interactions between the target and the two fragments of the projectile. For the scattering of ^{6,7}Li and ^{12}C, there was an attempt to obtain the interactions microscopically. However, some phenomenological treatments of the imaginary parts of the interactions were necessary in that period. Three-body CDCC thus had some limitations. After the review articles, CDCC has been developed in several aspects, and applied to various studies in wide research fields. The main purpose of the present article is to review these developments and applications of CDCC.

One of the most important developments is the construction of the microscopic reaction theory for nucleus-nucleus scattering62) based on the multiple scattering theory. This gives a foundation of CDCC and other reaction calculations that adopt microscopic nucleus-nucleus interactions based on the NN t or g matrix. The microscopic reaction theory is reduced to the double-folding model when both nuclear and

Coulomb breakup are weak. Then it allows us to practically obtain a microscopic optical potential. As mentioned above, CDCC is designed to accurately treat the breakup of a projectile into some fragments. The double-folding model can be used the input potentials of CDCC, i.e., the microscopic optical potential between the target and each constituent of the projectile.

In §2, we recapitulate the original version of CDCC, i.e., three-body CDCC, and show its theoretical foundation, with clarifying the relation between the Faddeev method and CDCC. In §3, we present the microscopic reaction theory for nucleus-nucleus scattering. We also discuss the validity of the Glauber model and examine the localization prescription by Brieva and Rook[63)] for the nonlocal microscopic optical potentials. The double-folding model is then applied to the scattering of stable nuclei and unstable Ne isotopes at intermediate energies, in which breakup effects are expected to be small. We propose in §4 eikonal-CDCC (E-CDCC) that treats Coulomb-dominated breakup processes very accurately and efficiently. Inclusion of dynamical relativistic effects in breakup reactions is also accomplished. In §5 we extend three-body CDCC to treat breakup processes of a projectile that has a three-body structure, i.e., four-body CDCC. We describe also how to smooth the discrete breakup cross sections obtained by CDCC. The eikonal reaction theory (ERT) is proposed in §6, which makes CDCC applicable to inclusive breakup reactions. CDCC and the extended theories are applied to the scattering of unstable nuclei in §7, to reactions essential in cosmology and astrophysics in §8, and to reactions concerning nuclear engineering in §9. Finally, we give summary in §10.

§2. Theoretical foundation of CDCC

In this section, we recapitulate the original version of CDCC,[24),25)] i.e., three-body CDCC, and show the theoretical foundation[64),65),66)] in order to understand what CDCC is.

2.1. *Three-body CDCC*

We consider the projectile that is composed of two particles b and c exactly or approximately. In this case, the scattering of the projectile on a target (A) can be described by the A+b+c three-body system. Figure 1 is an illustration of the three-body system and coordinates among the three particles. The three-body scattering is governed by the Schrödinger equation

$$[H-E]\Psi=0 \tag{2·1}$$

with the Hamiltonian

$$H=K_r+K_R+v(\boldsymbol{r})+U_{\rm b}(\boldsymbol{r}_{\rm b})+U_{\rm c}(\boldsymbol{r}_{\rm c}), \tag{2·2}$$

where K_r and K_R are the kinetic energy operators associated with $\boldsymbol{r}$ and $\boldsymbol{R}$, respectively, and $v(\boldsymbol{r})$ is the interaction between b and c, while $U_{\rm b}$ ($U_{\rm c}$) is an optical potential of the scattering of b (c) on A.

In CDCC, the total wave function Ψ is expanded by the complete set of eigenfunctions of the Hamiltonian $h=K_r+v(\boldsymbol{r})$ of the b+c subsystem. The eigenfunctions

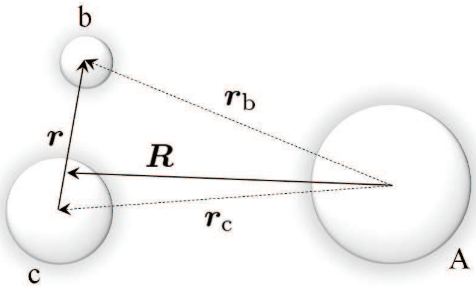

Fig. 1. Illustration of the A+b+c three-body system. Vector $\boldsymbol{r}_\gamma$ (γ =b or c) is the relative coordinate between γ and A, whereas $\boldsymbol{R}$ and $\boldsymbol{r}$ form a set of Jacobi coordinates.

are composed of bound and continuum states. The continuum states are characterized by the orbital angular momentum ℓ and the linear momentum k of the b+c subsystem, and they are truncated as

$$k \leq k_\mathrm{max}, \quad \ell \leq \ell_\mathrm{max}. \tag{2·3}$$

The ℓ- and k-truncations are the primary approximation in CDCC. After making the truncations, we further discretize the k-continuum. The model space $\mathcal{P}'$ thus constructed is described by

$$\mathcal{P}' = \sum_{i=0}^{N} |\phi_i\rangle\langle\phi_i|, \tag{2·4}$$

where the ϕ_i represent the bound and discretized-continuum states of h, and N is the number of the ϕ_i. The total wave function Ψ is hence approximated into

$$\Psi \approx \Psi_\mathrm{CDCC} \equiv \mathcal{P}'\Psi = \sum_{i=0}^{N} \phi_i(\boldsymbol{r})\chi_i(\boldsymbol{R}), \tag{2·5}$$

where the coefficients $\chi_i(\boldsymbol{R})$ of the expansion describe motions between the projectile in the states ϕ_i and A. The approximate total wave function Ψ_CDCC is obtained by solving the three-body Schrödinger equation (2·1) in the model space $\mathcal{P}'$

$$\mathcal{P}'[H - E]\mathcal{P}'\Psi_\mathrm{CDCC} = 0. \tag{2·6}$$

This leads to a set of coupled-channel equations for $\chi_i(\boldsymbol{R})$,

$$[E - K_R - \varepsilon_i]\chi_i(\boldsymbol{r}) = \sum_{j}^{N} \langle\phi_i|U|\phi_j\rangle\chi_j(\boldsymbol{R}), \tag{2·7}$$

where $U = U_\mathrm{b}(\mathbf{r}_\mathrm{b}) + U_\mathrm{c}(\mathbf{r}_\mathrm{c})$ and the ε_i are energies of the b+c subsystem in the ϕ_i. Solving the CDCC equations (2·7) with the ordinary boundary condition, one can get the S-matrix elements of the elastic scattering and the projectile-breakup reactions.$^{24),25)}$

As for the discretization prescription, three methods have been proposed so far: i) the average (Av) method,[24),25),59)] ii) the midpoint (Mid) method,[25),67),68)] and iii) the pseudo-state (PS) method.[24),54),69),47),49),48),50),57)] In the Av and Mid methods, the k-continuum is divided into a finite number of bins. In the Av method, the continuum states within each bin are averaged into a single state, whereas in the Mid method they are represented by a single state at a midpoint of the bin. The Av and Mid methods are valid, since the two methods yield the same converged S-matrix elements as the width $\varDelta$ of bins decreases.[67),68)] The Av method is more practical than the Mid one, because the former requires less numerical tasks than the latter. Since then the Av method has widely been used as a standard way of the discretization.

In the PS method, on the other hand, h is diagonalized in a space spanned by a finite number of L^2-type basis functions. The resulting eigenstates can be regarded as bound states when the eigenenergies are negative and as discretized-continuum states when the eigenenergies are positive. The discretized-continuum states are thus obtained by a superposition of analytic basis functions in the PS method. This makes numerical tasks much easier. We could not derive, however, a smooth breakup cross section from the discrete breakup cross section calculated with CDCC. For this reason, the PS method was applied to virtual breakup processes in the intermediate state of elastic scattering and transfer reactions, but not to breakup reactions themselves. This problem has recently been solved by the smoothing method proposed in Refs. 47), 49), 48), 50). This smoothing method is presented in §5.

The S-matrix elements calculated with CDCC depend on the parameters, $\ell_{\rm max}$, $k_{\rm max}$, $\varDelta$, i.e., the size of the model space P'. This artifact should be removed by confirming that the calculated S-matrix elements converge as the model space is expanded. Indeed, the convergence was shown in Refs. 24), 25), 67), 68). The next question to be addressed is whether the converged S-matrix elements are exact. This point is discussed in the next subsection.

2.2. *Relation between CDCC and Faddeev solutions*

As mentioned in §2.1, CDCC is based on three approximations, the ℓ-truncation, the k-truncation, and the discretization of the k-continuum. The ℓ-truncation is most essential among these approximations as shown below. Now we introduce the projection operator $\mathcal{P}$ that only selects ℓ up to $\ell_{\rm max}$. Obviously, $\mathcal{P}'$ tends to $\mathcal{P}$ in the limit of large $k_{\rm max}$ and small $\varDelta$. The component $\mathcal{P}\varPsi$ has no asymptotic amplitudes in the rearrangement channels. For example, let us consider a simple case of $\ell_{\rm max} = 0$. Then, $\mathcal{P}U\mathcal{P}$ is the average of U over the angle of vector $\boldsymbol{r}$. After the angle average, the potential $\mathcal{P}U\mathcal{P}$ becomes a function of r and R. Thus, $\mathcal{P}U\mathcal{P}$ is a three-body potential that vanishes at large R and/or large r, so that it does not generate any rearrangement channel.

The insertion of three-body distorting potentials does not change the mathematical properties of the Faddeev equations.[70)] Now we consider $\mathcal{P}U\mathcal{P}$ as such a distorting potential in order to obtain the distorted Faddeev equations,

$$(E - K_r - K_R - v - \mathcal{P}U\mathcal{P})\psi_{\rm A} = v(\psi_{\rm b} + \psi_{\rm c}), \tag{2·8}$$

$$(E - K_r - K_R - U_{\rm b})\psi_{\rm b} = (U_{\rm b} - \mathcal{P}U_{\rm b}\mathcal{P})\psi_{\rm A} + U_{\rm b}\psi_{\rm c}, \tag{2·9}$$

$$(E - K_r - K_R - U_{\rm c})\psi_{\rm c} = (U_{\rm c} - \mathcal{P}U_{\rm c}\mathcal{P})\psi_{\rm A} + U_{\rm c}\psi_{\rm b}, \tag{2·10}$$

where $\psi_{\rm A}$, $\psi_{\rm b}$, and $\psi_{\rm c}$ satisfy the relation $\Psi = \psi_{\rm A} + \psi_{\rm b} + \psi_{\rm c}$. If Eqs. (2·8)–(2·10) are added, the distorting potential is canceled and the original three-body Schrödinger equation (2·1) is recovered. In an iterative approach to Eqs. (2·8)–(2·10), the zeroth-order solution for $\psi_{\rm A}$ is obtained by setting the right-hand side of Eq. (2·8) to zero. The zeroth-order solution is nothing but $\Psi_{\rm CDCC}$. When $\Psi_{\rm CDCC}$ is inserted in Eqs. (2·9) and (2·10), the equations do not generate any disconnected diagram, since $\Psi_{\rm CDCC}$ has no rearrangement channel in the asymptotic region. Furthermore, the subtractions, $U_{\rm b} - \mathcal{P}U_{\rm b}\mathcal{P}$ and $U_{\rm c} - \mathcal{P}U_{\rm c}\mathcal{P}$, sizably weaken couplings of $\Psi_{\rm CDCC}$ with $\psi_{\rm b}$ and $\psi_{\rm c}$. Thus, $\Psi_{\rm CDCC}$ is a good solution to the three-body Schrödinger equation (2·1), when $\ell_{\rm max}$ is large enough. Very lately, the CDCC solution has directly been compared with the Faddeev solution through numerical calculations and it has been shown that the two solutions agree very well with each other.[66)]

The discussion mentioned above is made without using the k-truncation and the discretization of k-continuum. The ℓ-truncation is thus most essential in CDCC.

§3. Microscopic reaction theory for nucleus-nucleus scattering

In this section, we present a microscopic reaction theory for nucleus-nucleus scattering, following Ref. 62). The validity of the Glauber model is discussed with the microscopic reaction theory. When the projectile breakup is weak, the theory is reduced to the double-folding model with the effective nucleon-nucleon (NN) interaction. The microscopic optical potential constructed with the double-folding model is applied to measured reaction cross sections for the scattering of stable nuclei and neutron-rich Ne isotopes around 240 MeV/nucleon. Through the analyses, it is confirmed that the microscopic optical potential is reliable and hence can be used in CDCC as the potentials between a target and fragments of a projectile. This microscopic version of CDCC can be applied to many nucleus-nucleus scattering.

3.1. *Microscopic reaction theory*

The most fundamental equation to describe nucleus-nucleus scattering is the many-body Schrödinger equation with the realistic NN interaction v_{ij}

$$(K + h_{\rm P} + h_{\rm A} + \sum_{i\in{\rm P}, j\in{\rm A}} v_{ij} - E)\Psi^{(+)} = 0, \tag{3·1}$$

where E is the energy of the total system, K is the kinetic-energy operator for the relative motion between a projectile (P) and a target (A), and $h_{\rm P}$ ($h_{\rm A}$) is the internal Hamiltonian of P (A). The scattering of P from A can be described with a series of multiple scattering in terms of v_{ij}. In the series, one can first take a summation of ladder diagrams between the same NN pair. The summation can be described by an effective NN interaction τ_{ij} in nuclear medium. Taking a resummation of the series in terms of τ_{ij}, one can get the many-body Schrödinger equation with τ_{ij}[62]

$$(K + h_{\rm P} + h_{\rm A} + \sum_{i\in{\rm P},j\in{\rm A}} \tau_{ij} - E)\hat{\Psi}^{(+)} = 0 , \tag{3·2}$$

where it has been assumed that the number of pairs (i, j) is much larger than unity. We further assumed that the antisymmetrization between incident nucleons in P and target nucleons in A can be approximated by using τ_{ij} that is properly antisymmetrical with respect to the exchange of the colliding nucleons. The first assumption is satisfied well for nucleus-nucleus scattering, and the second one is known to be accurate at intermediate and high incident energies.[71],[72] This is an extension of the Kerman-McManus-Thaler formalism[14] for nucleon-nucleus scattering to nucleus-nucleus scattering.

As mentioned above, τ_{ij} describes nucleon-nucleon scattering in nuclear medium. A possible simplification of τ_{ij} is to replace τ_{ij} with the Brückner g-matrix interaction, which has been done in many applications; see, e.g., Refs. 63), 73), 74), 75), 76), 77), 78), 79), 80). The g-matrix interaction, however, does not include effects induced by finite nucleus, e.g., effects of projectile breakup and target collective excitations, because the interaction is evaluated in infinite nuclear matter. In other words, τ_{ij} is much more complicated than the g-matrix interaction. Therefore, in general, it is not easy to solve the many-body Schrödinger equation (3·2). However, it becomes feasible at least in the following cases.

First, if we consider a) nucleus-nucleus scattering at high incident energies, or, b) scattering of lighter projectiles from lighter targets at intermediate incident energies, effects induced by finite nucleus such as projectile breakup and target collective excitations are small. Then, the double-folding model becomes reliable, with which we can analyze the elastic-scattering cross section or the total reaction cross section $\sigma_{\rm R}$. We discuss the validity of the double-folding model for the scattering of type b) in §3.4 and §3.5. It should be noted that in this case the Glauber model also becomes reliable, since Coulomb breakup is negligible. The observables to be analyzed with the Glauber model are $\sigma_{\rm R}$ or inclusive cross sections such as the one-neutron removal cross section. The validity of the Glauber model is discussed in §3.2.

Second, let us consider a projectile that is a weakly bound system of two nucleus b and c. Then the many-body Schrödinger equation (3·2) is approximated well into the three-body Schrödinger equation (2·1), in which the potential $U_\gamma(\boldsymbol{r}_\gamma)$ (γ =b or c) is constructed to reproduce the scattering of γ on A. When γ is not a weakly bound system, the potential can be constructed microscopically with the double-folding model, i.e., by folding the effective NN interaction with the densities of A and γ. Thus, we can solve with high accuracy Eq. (3·2) by three-body CDCC with all the input optical potentials obtained microscopically. Note that the microscopic potential is nonlocal in general, which makes it very difficult to solve Eq. (2·1). It is, however, possible to derive a local potential equivalent to the nonlocal potential by using the method proposed by Brieva and Rook.[63] The validity of their localization method is discussed in §3.3.

3.2. *Validity of the Glauber model*

The Glauber model is based on the eikonal approximation for NN scattering and the eikonal and adiabatic approximations for nucleus-nucleus scattering. The condition for the eikonal approximation to be good for NN collisions in both free space and nucleus-nucleus scattering is that

$$v(\boldsymbol{r})/e \ll 1, \quad ka \gg 1, \tag{3·3}$$

where e (k) is the kinetic energy (wave number) of the NN collision, $\boldsymbol{r}$ is the relative coordinate between two nucleons and a is the range of the realistic NN interaction v. Obviously, this condition is not well satisfied, because v has a strong short-range repulsive core; for example, $v \sim 2,000$ MeV at $r = 0$ for the AV18 force.$^{81)}$ In fact, the eikonal approximation is not good for NN scattering at intermediate energies, as shown in the left panel of Fig. 2. To avoid this problem, a slowly-varying function such as the Gaussian form has been used as a profile function in the Glauber model.$^{82)}$

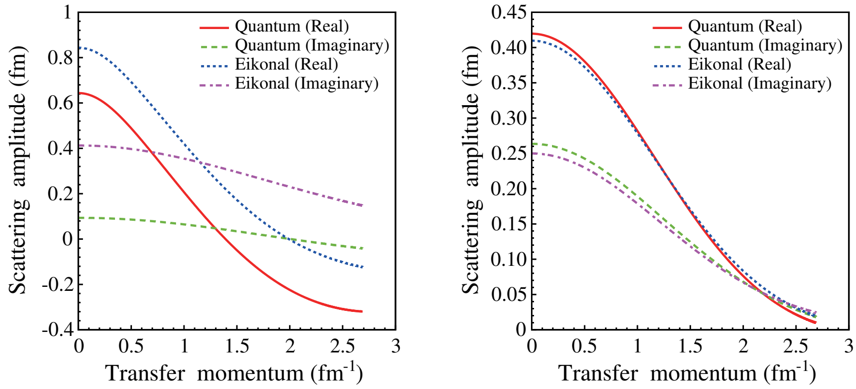

Fig. 2. The on-shell NN scattering amplitude $f_{\rm NN}(\boldsymbol{q})$ at the laboratory energy $E_{\rm NN} = 150$ MeV calculated with the bare NN potential AV18 in the left panel and with the JLM g matrix$^{74)}$ in the right panel. The solid (dashed) and dotted (dash-dotted) lines show, respectively, the real and imaginary parts of $f_{\rm NN}(\boldsymbol{q})$ of the exact (eikonal) calculation.

The use of a slowly-varying profile function and hence of a slowly-varying NN interaction can be justified by using the many-body Schrödinger equation (3·2). Applying the adiabatic and eikonal approximations to Eq. (3·2), one can obtain the S matrix of nucleus-nucleus scattering as

$$S = \exp\Big[-\frac{i}{\hbar v_{\rm rel}} \sum_{ij} \int_{-\infty}^{\infty} dz_{ij} \tau_{ij} \Big], \tag{3·4}$$

where $v_{\rm rel}$ stands for a velocity of P relative to A and z_{ij} is the z-component of the relative coordinate $\boldsymbol{r}_{ij}$ between two nucleons. In general, τ_{ij} has much milder r dependence than the bare NN potential v_{ij}. At high incident energies, for instance, τ_{ij} is reduced to the t matrix of NN scattering that is a product of v_{ij} and the wave operator of the NN scattering. When v_{ij} has a strong repulsive core at small r, the wave operator provides a large suppression there. This leads to the fact that the t matrix is a slowly-varying function of r.[62] This is also the case with the g matrix. The t- or g-matrix is thus more suitable than v_{ij} as an input of the Glauber model. In fact, as shown in the right panel of Fig. 2, the eikonal approximation is quite good for NN scattering at intermediate energies, say, 150 MeV, when the g matrix proposed by Jeukenne, Lejeune, and Mahaux (JLM)[74] is adopted. The use of the g-matrix interaction has another merit in the sense that the effective interaction includes, at least in part, nuclear medium effects.

3.3. *Localization of nonlocal microscopic optical potential*

In this subsection, we focus our discussion on nucleon-nucleus scattering for simplicity. The multiple scattering theory proposed by Watson[13] was reformulated by Kerman, McManus, and Thaler[14] as series expansion in terms of an underlying NN t matrix. The expansion was developed as the spectator expansion,[83] and the corresponding first-order optical potential was successful in reproducing experimental data in a wide range of incident energies $E_{\rm in}$ from 65 MeV to 400 MeV.[84] The microscopic optical potential thus produced is complex and nonlocal.

Another way of obtaining the microscopic optical potential is the single-folding model with the g-matrix interaction.[63],[73],[74],[75],[76],[77],[78],[79],[80] The g-matrix interaction is evaluated in infinite nuclear matter, and the potential between an incident nucleon and a target is constructed by folding the g-matrix interaction with the target density by using the local-density approximation. This approach also is highly successful in reproducing nucleon-nucleus elastic scattering data[79],[85] for 40 MeV $< E_{\rm in} <$ 800 MeV from light to heavy targets. The optical potential constructed in this approach is, again, complex and nonlocal.

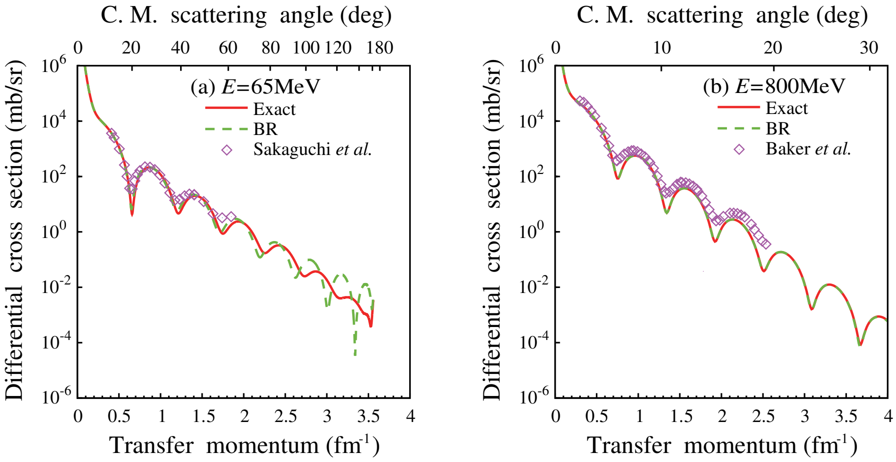

Fig. 3. The differential cross sections of the proton elastic scattering from ^{90}Zr at (a) 65 MeV and (b) 800 MeV. The lower (upper) horizontal scale shows the transferred wave number q (the scattering angle $\theta_{\rm cm}$). The solid curves represent the results of the exact calculation, whereas the dashed lines correspond to those of the equivalent local potential. Experimental data are taken from Refs. 86) and 87).

Thus, there have been several works on microscopic optical potentials. The use of a nonlocal optical potential is, however, not practical in many applications. This is true also in CDCC calculations, since the nonlocality makes it difficult to solve the CDCC equation (2·7). In Ref. 63), Brieva and Rook proposed an approximate form of the equivalent local potential. This Brieva-Rook (BR) localization has then been commonly used in many studies,$^{78),77),80)}$ the accuracy of which has not yet been examined numerically.

In Ref. 88), we tested the validity of the BR localization for the proton elastic scattering from ^{90}Zr in a wide range of incident energies from 65 to 800 MeV. As shown in Fig. 3, the BR localization works very well for $q \lesssim 2$ fm^{-1} at 65 MeV and for $q \lesssim 4$ fm^{-1} at 800 MeV. The BR localization is thus accurate in a wide range of $65 \lesssim E_{\rm in} \lesssim 800$ MeV, unless q is large.

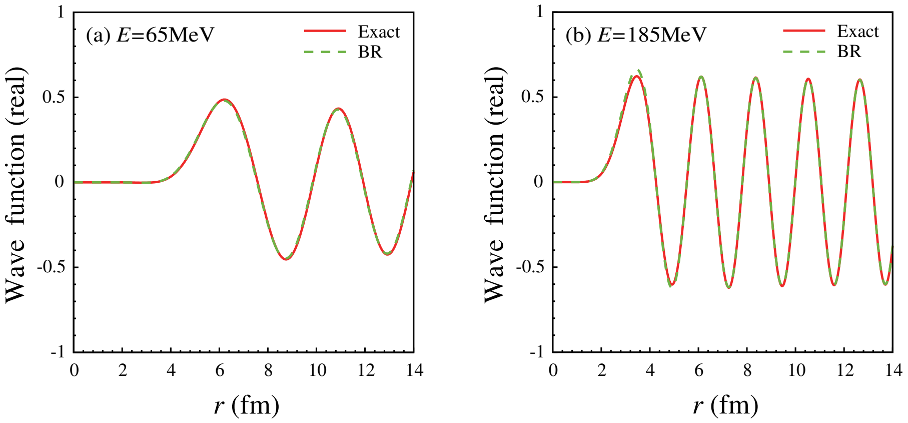

Fig. 4. The real part of the exact and approximate wave functions for the p+^{90}Zr scattering at the grazing angular momentum. See the text for details.

In Fig. 4, the real part of the exact wave function (solid line) of the Schrödinger equation with the nonlocal microscopic potential is compared with that of the approximate wave function (dashed line) calculated with the equivalent local potential for the p+^{90}Zr scattering at the grazing angular momentum. For both $E_{\rm in} = 65$ MeV (left panel) and 185 MeV (right panel), the two results agree very well with each other. The exact wave function is thus not suppressed at small R by the nonlocality of the optical potential, i.e., the Perrey suppression factor$^{89)}$ is not necessary in the BR-type localization.

3.4. *Application of the double-folding model to the scattering of stable nuclei*

In this subsection, we consider the scattering of stable nuclei from lighter targets at intermediate energies. Then, projectile breakup and collective target excitations are considered to be small, and consequently, the double-folding model becomes reliable. In the double-folding model, the potential U is obtained as a sum of the direct part $U^{\rm DR}$ and the exchange part $U^{\rm EX}$[90),91)]

$$U^{\rm DR}(\boldsymbol{R}) = \sum_{\mu,\nu} \int \rho_{\rm P}^{\mu}(\boldsymbol{r}_{\rm P})\rho_{\rm A}^{\nu}(\boldsymbol{r}_{\rm A})g_{\mu\nu}^{\rm DR}(s;\rho_{\mu\nu})d\boldsymbol{r}_{\rm P}d\boldsymbol{r}_{\rm A}, \tag{3·5}$$

$$\begin{aligned} U^{\rm EX}(\boldsymbol{R}) = \sum_{\mu,\nu} \int & \rho_{\rm P}^{\mu}(\boldsymbol{r}_{\rm P},\boldsymbol{r}_{\rm P}-\boldsymbol{s})\rho_{\rm A}^{\nu}(\boldsymbol{r}_{\rm A},\boldsymbol{r}_{\rm T}+\boldsymbol{s}) \\ & \times g_{\mu\nu}^{\rm EX}(s;\rho_{\mu\nu})\exp\left[-i\boldsymbol{K}(\boldsymbol{R})\cdot\boldsymbol{s}/M\right]d\boldsymbol{r}_{\rm P}d\boldsymbol{r}_{\rm A} \end{aligned} \tag{3·6}$$

with $\boldsymbol{s}=\boldsymbol{r}_{\rm P}-\boldsymbol{r}_{\rm A}+\boldsymbol{R}$. The relative coordinate between P and A is denoted by $\boldsymbol{R}$, and $\boldsymbol{r}_{\rm P}$ ($\boldsymbol{r}_{\rm A}$) is the coordinate of a nucleon in P (A) from the center-of-mass (c.m.) of P (A); μ (ν) stands for the z-component of the isospin of a nucleon in P (A). The original form of $U^{\rm EX}$ is nonlocal, but it has been localized in Eq. (3·6) with the BR localization, where $M = A_{\rm P}A_{\rm A}/(A_{\rm P}+A_{\rm A})$ with $A_{\rm P}$ ($A_{\rm A}$) the mass number of P (A). The direct part $g_{\mu\nu}^{\rm DR}$ and the exchange part $g_{\mu\nu}^{\rm EX}$ of the g matrix are assumed to depend on the local density

$$\rho_{\mu\nu} = \rho_{\rm P}^{\mu}(\boldsymbol{r}_{\rm P}-\boldsymbol{s}/2)+\rho_{\rm A}^{\nu}(\boldsymbol{r}_{\rm A}+\boldsymbol{s}/2) \tag{3·7}$$

at the midpoint of the interacting nucleon pair. As for the projectile density $\rho_{\rm P}^{\mu}$ and the target density $\rho_{\rm A}^{\nu}$, we use the phenomenological proton-density[92)] deduced from electron scattering, and assume that the neutron density has the same geometry as the corresponding proton one, since the root-mean-square radii of proton and neutron agree with each other with more than 99% accuracy in the Hartree-Fock (HF) calculation.

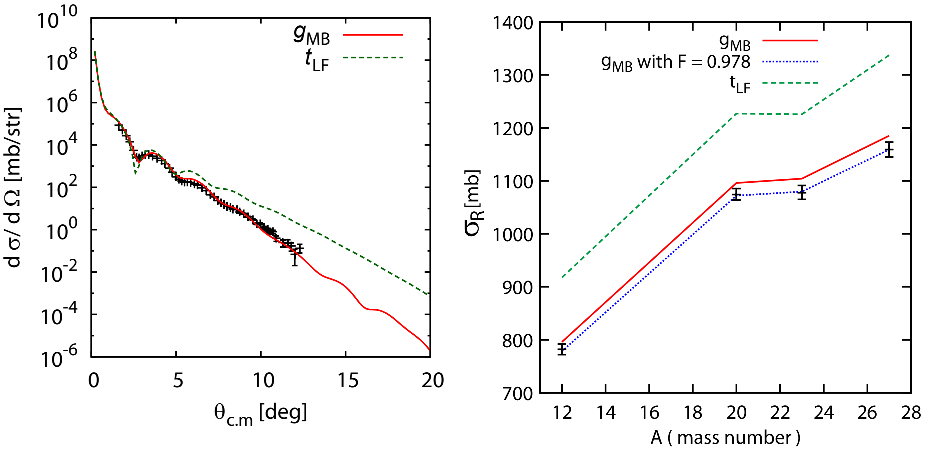

Fig. 5. Angular distribution of the ^{12}C+^{12}C elastic cross section at 135 MeV/nucleon (left panel) and reaction cross sections for ^{12}C scattering from ^{12}C, ^{20}Ne, ^{23}Na, and ^{27}Al (right panel). In each panel, the solid (dashed) line shows the result with $g_{\rm MB}$ ($t_{\rm LF}$). The dotted line in the right panel represents the result with $g_{\rm MB}$ multiplied by 0.978. The experimental data are taken from Ref. 93) (left panel) and Refs. 11),95),96),97) (right panel).

We show in the left panel of Fig. 5 the angular distribution of the ^{12}C+^{12}C elastic scattering at 135 MeV/nucleon. The folding model calculation with the Melbourne

g matrix ($g_{\rm MB}$) reproduces well the data,[93] whereas that with the Love-Franey t-matrix interaction ($t_{\rm LF}$)[94] does not. The medium effect is thus important, and the double-folding model with $g_{\rm MB}$ is found to be quite reliable at intermediate incident energies. The right panel shows reaction cross sections $\sigma_{\rm R}$ for ^{12}C scattering from ^{12}C, ^{20}Ne, ^{23}Na, and ^{27}Al targets at 250.8 MeV/nucleon. The solid and dotted lines represent the results of folding model calculations with $g_{\rm MB}$ before and after the normalization of $F = 0.978$, respectively. Before the normalization procedure, the results (solid line) slightly overestimate the mean values of the experimental data[11],[95],[96],[97] for $A = 20$–27. After the normalization, the results (dotted line) agree with the mean values for all the targets. The dashed line corresponds to the results of double-folding model calculations with $t_{\rm LF}$ and no normalization. One sees clearly that the medium effect on $\sigma_{\rm R}$ is also significant at this energy.

3.5. *Application of the double-folding model to reaction cross sections for Ne isotopes*

In this subsection, the double-folding model is applied to the scattering of Ne isotopes from a ^{12}C target at 240 MeV/nucleon. The projectile densities are constructed by either (I) antisymmetrized molecular dynamics (AMD)[98] with the Gogny D1S interaction[99],[100] or (II) the deformed Woods-Saxon (DWS) model with the deformation evaluated by AMD.

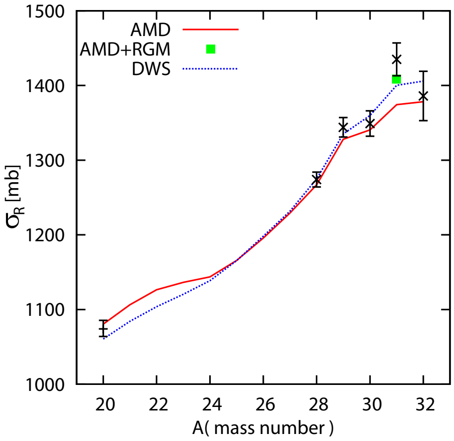

Fig. 6. Reaction cross sections for the scattering of Ne isotopes from a ^{12}C target at 240 MeV/nucleon. The experimental data are taken from Refs. 11) and 96). The dotted line represents the result of the DWS model (method II), whereas the solid line corresponds to the result of AMD calculations (method I). The closed square represents the result of the AMD-RGM calculation.

Figure 6 represents the $\sigma_{\rm R}$ for the scattering of Ne isotopes from a ^{12}C target at 240 MeV/nucleon. The result of the double-folding model with the AMD density (method I) shown by the solid line reproduces well the data[11] except for ^{31}Ne. It turns out that deformation effects give a significant increase in the $\sigma_{\rm R}$ and thus very important for the reproduction of the data; even no bound state is obtained with a spherical HF calculation for $A > 30$.

The underestimation of method I for ^{31}Ne comes from the inaccuracy of the AMD density in its tail region. To remove this shortcoming, we describe the ground state of ^{31}Ne by a ^{30}Ne+n cluster model including several configurations of the valence neutron as well as excited states of ^{30}Ne below 10 MeV. We adopt the resonating group method (RGM) to include antisymmetrization of nucleons explicitly.101) The result of this AMD-RGM calculation is shown by the square symbol, which reproduces well the experimental data11) with no adjustable parameter. It is found that the tail correction gives an increase in $\sigma_{\rm R}$ by 35 mb. From these findings, we conclude that ^{31}Ne is a halo nucleus with large deformation.

Although the AMD-RGM calculation is highly successful, it is quite time consuming. Thus, the DWS model (method II) becomes an important alternative. As shown by the dotted line, method II simulates well the results of method I for $A \neq 31$ and the result of AMD-RGM for $A = 31$. An important advantage of method II is that the tail correction mentioned above is not necessary. This suggests that the DWS model is a handy and promising way of simulating the AMD model with the tail correction. The difference between method I and method II for $^{28-32}$Ne may show the tail correction to method I.

Further investigations on effects of breakup, dynamical deformation, and reorientation were made in Refs. 102) and 103). The findings obtained on $\sigma_{\rm R}$ for the ^{30,31}Ne+^{12}C scattering at 240 MeV/nucleon are summarized as follows.

1) The breakup effects of ^{31}Ne to ^{30}Ne+n is 0.7%.
2) Coupled-channel effects due to the deformation, i.e., couplings to the rotational states, of ^{30}Ne is less than 1%.
3) Difference between $\sigma_{\rm R}$ and the interaction cross section $\sigma_{\rm I}$, i.e., the total inelastic cross section, is 0.2% for ^{30}Ne.
4) The reorientation effect due to the intrinsic spin of ^{31}Ne($3/2^-$) is 0.2%.

Thus, these so-called higher-order effects on $\sigma_{\rm R}$ are found to be very small for the present reaction systems. It should be noted, however, that an elastic breakup or inelastic excitation to a rotational state itself is an interesting subject of nuclear physics. Then, CDCC or ordinary coupled-channel calculation for these processes will be necessary. Nevertheless, as mentioned in §3.1, the microscopic reaction theory constructed is indispensable, because it gives a theoretical foundation as well as input potentials to these reaction calculations.

§4. Proposal of eikonal-CDCC (E-CDCC) as a method of treating Coulomb breakup

For some decades, Coulomb breakup (or Coulomb excitation) processes have been regarded as one of the most effective tools to investigate nuclear properties.104) The standard theory to describe such processes is the virtual photon theory (VPT),105),106) or sometimes called equivalent photon method, which is based on the picture that a nucleus moves along with its classical trajectory, and dissociates by the electromagnetic field constructed by the target nucleus. Although the VPT has been highly successful in many cases, various higher-order processes that are not included in the VPT can play some important roles, i.e., nuclear breakup, interference between nuclear and Coulomb amplitudes, and multistep breakup processes mainly due to strong continuum-continuum couplings, and so forth. Quantitative evaluation of these contributions with more sophisticated quantum mechanical models is very important for genuine understanding of the "Coulomb" breakup processes.

The first application of CDCC to Coulomb breakup was done by Hirabayashi and Sakuragi[28)] for ^{208}Pb(^{6}Li,α+d) at 156 MeV. Later CDCC analyses of ^{58}Ni(^{8}B,^{7}Be+p) at 26 MeV[36)] and ^{208}Pb(^{8}B,^{7}Be+p) at 44 and 83 MeV/nucleon[37)] were performed. The most essential characteristic of these CDCC calculations is that the number of partial waves, $L_{\max}$, between the projectile (P) and the target (A) is extremely large; typically, $L_{\max} = 15,000$ was taken in Ref. 37). This is due to the very long-range Coulomb coupling potentials, the dipole components in particular. These calculations definitely show the applicability of CDCC to Coulomb breakup processes. However, inclusion of such large numbers of partial waves is time-consuming and requires very careful numerical treatment of the coupled-channel calculations.

In Ref. 45) we proposed a new framework for accurately and efficiently describing Coulomb breakup processes, i.e., *eikonal-CDCC (E-CDCC).* Let us consider a reaction system of P and A, in which P consisting of a core nucleus (c) and a valence particle (b). E-CDCC uses the Coulomb-eikonal approximation to the scattering waves between P and A. Consequently, the wave function of the three-body system is given by

$$\varPsi(\boldsymbol{R},\boldsymbol{r}) = \sum_c \varPhi_c(\boldsymbol{r}) e^{-i(m-m_0)\phi_R}\psi_c(b,z)\phi^{\rm C}_{\boldsymbol{K}_c}(b,z), \tag{4·1}$$

where $\varPhi_c(\boldsymbol{r})$ is the internal wave function of P with c the channel indices $\{i,\, \ell,\, m\}$; $i > 0$ ($i = 0$) stands for the ith discretized-continuum (ground) state, and ℓ and m are, respectively, the orbital angular momentum between the constituents (c and b) of P and its projection on the z-axis taken to be parallel to the incident beam. m_0 is the value of m in the incident channel. We here neglect the internal spins of c and b for simplicity; see Ref. 46) for the inclusion of the intrinsic spins of P in the E-CDCC formalism. b is the impact parameter (or transverse coordinate) in the collision of P and A, which is defined by $b = \sqrt{x^2+y^2}$ with $\boldsymbol{R} = (x,y,z)$, the relative coordinate of P from A in the Cartesian representation. Note that $\varPsi(\boldsymbol{R},\boldsymbol{r})$ properly takes into account the dependence of the wave function on the azimuthal angle ϕ_R around the z-axis, which corresponds to the *coherent choice* of the wave function in the terminology of the dynamical eikonal approximation (DEA).[60),61)]

The use of the Coulomb incident wave $\phi^{\rm C}_{\boldsymbol{K}_c}(b,z)$ instead of the plane wave $\exp(\boldsymbol{K}_c \cdot \boldsymbol{R})$ in the eikonal approximation is one of the most important features of E-CDCC; $\boldsymbol{K}_c$ is the asymptotic wave-number vector of P in channel c from A. In actual calculations we use the following approximate asymptotic form

$$\phi^{\rm C}_{\boldsymbol{K}_c}(b,z) \approx \frac{1}{(2\pi)^{3/2}} e^{i(K_c z + \eta_c \ln{(K_c R - K_c z)})}, \tag{4·2}$$

which is valid for large values of b, with η_c the Sommerfeld parameter for channel c. We further assume

$$\boldsymbol{\nabla}_{\boldsymbol{R}} \phi^{\rm C}_{\boldsymbol{K}_c}(b,z) \approx iK_c(R)\phi^{\rm C}_{\boldsymbol{K}_c}(b,z)\frac{\boldsymbol{z}}{z} \tag{4·3}$$

with

$$K_c(R)=\sqrt{K_c^2-\frac{2\mu_R}{\hbar^2}\frac{Z_{\rm P}Z_{\rm A}e^2}{R}}, \tag{4·4}$$

where μ_R is the reduced mass of P and A, and $Z_{\rm P}e$ ($Z_{\rm A}e$) is the charge of P (A).

As in the usual eikonal approximation, the wave function $\psi_c(b,z)$ is assumed to be a slowly varying function and its second-order derivative $\Delta_{\boldsymbol{R}}\psi_c(b,z)$ is negligibly small. Then we obtain the following coupled-channel equations

$$\frac{i\hbar^2}{\mu_R}K_c^{(b)}(z)\frac{d}{dz}\psi_c^{(b)}(z)=\sum_{c'}\mathfrak{F}_{cc'}^{(b)}(z)\;\mathcal{R}_{cc'}^{(b)}(z)\;\psi_{c'}^{(b)}(z)\;e^{i(K_{c'}-K_c)z}, \tag{4·5}$$

where $\mathcal{R}_{cc'}^{(b)}(z)=(K_{c'}R-K_{c'}z)^{i\eta_{c'}}/(K_cR-K_cz)^{i\eta_c}$. The reduced coupling potential $\mathfrak{F}_{cc'}^{(b)}(z)$ is given by

$$\mathfrak{F}_{cc'}^{(b)}(z)=\langle\Phi_c|U_{\rm c}+U_{\rm b}|\Phi_{c'}\rangle_{\boldsymbol{r}}\,e^{i(m-m')\phi_R}-\frac{Z_{\rm P}Z_{\rm A}e^2}{R}\delta_{cc'}, \tag{4·6}$$

where $U_{\rm c}$ ($U_{\rm b}$) is the sum of the nuclear and Coulomb interactions between c (b) and A. The explicit form of the coupling potential is given in Refs. 45) and 46). Note that in Eq. (4·5) b is relegated to a superscript since it is not a dynamical variable.

Solving Eq. (4·5) under the boundary condition

$$\lim_{z\to-\infty}\psi_c^{(b)}(z)=\delta_{c0}, \tag{4·7}$$

where 0 denotes the incident channel, one obtains the following form of the eikonal scattering amplitude[45)]

$$f_{c0}^{\rm E}=f^{\rm Ruth}\delta_{c0}+\frac{2\pi}{iK_0}\sum_L f_{L;c0}^{\prime\rm E}\;Y_{L\,m-m_0}(\hat{\boldsymbol{K}}_c'), \tag{4·8}$$

where $f^{\rm Ruth}$ is the Rutherford amplitude. The partial scattering amplitude $f_{L;c0}^{\prime\rm E}$ is defined by

$$f_{L;c0}^{\prime\rm E}=\frac{K_0}{K_c}\mathcal{H}_c^{(b_{c;L})}\sqrt{\frac{2L+1}{4\pi}}i^{(m-m_0)}\left[\mathcal{S}_{c0,L}-\delta_{c0}\right], \tag{4·9}$$

where

$$\mathcal{S}_{c0,L}\equiv\lim_{z\to\infty}\psi_c^{(b_{c;L})}(z) \tag{4·10}$$

with $b_{c;L}\equiv(L+1/2)/K_c$. The eikonal Coulomb-phase factor $\mathcal{H}_{c,L}$ is defined by

$$\mathcal{H}_{c,L}=\exp[2i\eta_c\ln{(L+1/2)}]. \tag{4·11}$$

It should be noted that in the derivation of Eq. (4·8), we have used

$$\int_0^{2\pi}e^{-iM\phi_R}e^{-iK_cb_{c;L}\theta\cos\phi_R}d\phi_R=\frac{2\pi}{i^M}J_M((L+1/2)\theta)\approx 2\pi i^M\sqrt{\frac{4\pi}{2L+1}}Y_{LM}(\theta,0), \tag{4·12}$$

with assuming $L \gg 1$ and small scattering angles θ. Note also that $\eta_c \ln(L+1/2)$ in the exponent of $\mathcal{H}_{c,L}$ is the asymptotic form of the Coulomb phase shift $\sigma_L(\eta_c)$, i.e.,

$$\sigma_L(\eta_c) \to \eta_c \ln(L+1/2) \quad (\text{for } L \gg \eta_c). \tag{4·13}$$

Furthermore, the formal solution to Eq. (4·5) will be used as the starting equation of the eikonal reaction theory (ERT) described in §6.

The quantum mechanical (QM) correction in the scattering amplitude can be performed if one replaces $f'^{\rm E}_{L;c0}$ for small L, say, $L < L_{\rm C}$, with the QM partial amplitude obtained by conventional QM CDCC,

$$\begin{aligned} f'^{\rm Q}_{L;c0} \equiv \sum_{J=|L-\ell|}^{L+\ell} \sum_{L_0=|J-\ell_0|}^{J+\ell_0} \sqrt{\frac{2L_0+1}{4\pi}} (\ell_0 m_0 L_0 0|J m_0)(\ell m L\, m_0{-}m|J m_0) \\ \times (S^J_{iL\ell,i_0L_0\ell_0} - \delta_{ii_0}\delta_{LL_0}\delta_{\ell\ell_0}) e^{i(\sigma_L+\sigma_{L_0})}(-)^{m-m_0}, \end{aligned} \tag{4·14}$$

where J is the total angular momentum of the three-body system and S is the scattering matrix. This correction is valid if $f'^{\rm E}_{L;c0} \approx f'^{\rm Q}_{L;c0}$ with high precision for $L \geq L_{\rm C}$; this is in fact the definition of $L_{\rm C}$. We show how this is satisfied below (see Fig. 8). Thus, we use the following *hybrid* scattering amplitude

$$f_{c0} = f^{\rm Ruth}\delta_{c0} + \frac{2\pi}{iK_0}\sum_{L<L_{\rm C}} f'^{\rm Q}_{L;c0}\, Y_{L\,m-m_0}(\hat{\boldsymbol{K}}'_c) + \frac{2\pi}{iK_0}\sum_{L\geq L_{\rm C}} f'^{\rm E}_{L;c0}\, Y_{L\,m-m_0}(\hat{\boldsymbol{K}}'_c), \tag{4·15}$$

which enables one to perform coupled-channel calculations for Coulomb and nuclear breakup processes with high computational speed, freely from numerical difficulties due to extremely large values of L, and with the same accuracy as of conventional QM CDCC.

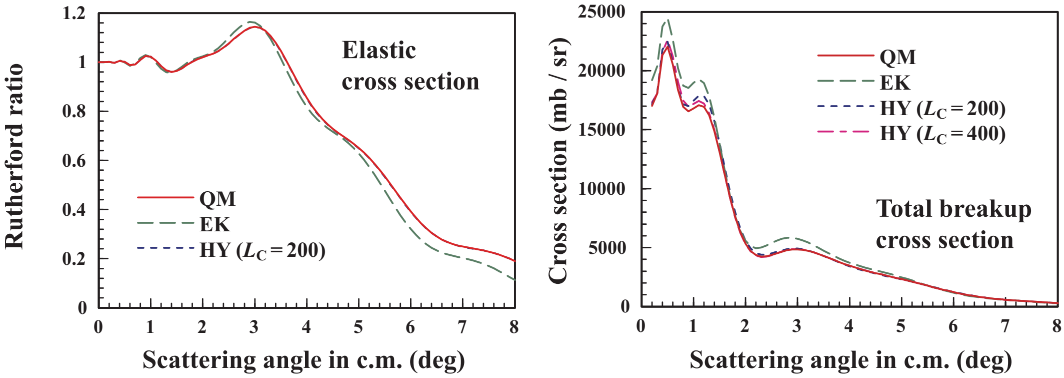

Fig. 7. Angular distribution of the elastic (left panel) and total breakup (right panel) cross sections for the ^{8}B+^{58}Ni scattering at 240 MeV. The solid and dashed lines show, respectively, the results of the QM and eikonal calculations. The dotted (dash-dotted) line represents the hybrid result with $L_{\rm C} = 200$ (400).

In the left and right panels of Fig. 7, respectively, we show the elastic cross section (Rutherford ratio) and the total breakup cross section for the ^{8}B+^{58}Ni scattering at

240 MeV (30 MeV/nucleon), as a function of the scattering angle θ in the center-of-mass (c.m.) frame. Details of the numerical inputs are given in Ref. 45); we here remark only that $L_{\max} = 4,000$ is taken in the calculation. The solid, dashed, and dotted lines represent the results of the QM, eikonal, and hybrid calculations, where $L_{\rm C}$ is taken to be 4,000, 0, and 200, respectively. In the right panel the result of the hybrid calculation with $L_{\rm C} = 400$ is also shown by the dash-dotted line. The hybrid calculations with an appropriate value of $L_{\rm C}$, namely, 200 (400) for the elastic (breakup) cross section, agree very well with the QM results; the difference is only less than 1%. Another interesting finding is that the difference between the QM and eikonal calculations is quite small up to even $\theta = 8^\circ$. This encourages one to use the eikonal approximation in analysis of reactions around 30 MeV/nucleon. If very high accuracy is required as in the study on determination of the astrophysical factor S_{17}, however, inclusion of the QM correction for lower partial waves is necessary (see §8.1). In any case, use of the eikonal amplitude is very effective to save computational time and eliminate numerical difficulties.

It is well known that a theoretical description of breakup reactions at intermediate energies requires a relativistic treatment of the reaction dynamics, though only a relativistic modification on the kinematics has been usually included. In Refs. 107) and 108), we developed a full coupled-channel calculation including a relativistic treatment of not only the kinematics but also the dynamics, based on E-CDCC. An essential ingredient of the relativistic coupled-channel calculation is the proper treatment of nuclear and Coulomb coupling potentials between P and A. We adopt the form of the Coulomb dipole and quadrupole interactions shown in Ref. 109), which is obtained from a relativistic Liénard-Wiechert potential with so-called far-field approximation; the validity of this approximation is confirmed in Ref. 108). As for the nuclear potential, the conjecture of Feshbach and Zabek[110)] is adopted.

It should be noted that E-CDCC can easily incorporate the relativistic Coulomb and nuclear coupling potentials, because it adopts the cylindrical coordinate representation. On the other hand, inclusion of these potentials in conventional CDCC, which is based on a partial wave decomposition in the spherical coordinate representation, is very complicated. Fortunately, however, the dynamical relativistic corrections are found to be necessary only for large L, where the scattering processes are described well by the eikonal approximation.

Figure 8 shows the real part of the breakup amplitude for ^{8}B+^{208}Pb at 250 MeV/nucleon as a function of L. As a breakup channel, we choose the s-wave 6th bin state, whose breakup amplitude has the largest value. For more details of numerical input, see Ref. 108). The solid line represents the result of nonrelativistic QM CDCC, which adopts Eq. (4·14) for all L and has no dynamical relativistic corrections. The dotted and dashed lines are the results of E-CDCC, based on Eq. (4·8), with and without dynamical relativistic corrections, respectively. One sees from the figure that at small L, i.e., $L \lesssim 300$, the dashed and dotted lines agree very well with each other, and deviate from the solid line. On the other hand, at large L, the solid and dashed lines show a very good agreement, as desired, and differ from the dotted line. Thus, using the amplitude obtained by nonrelativistic QM CDCC for small

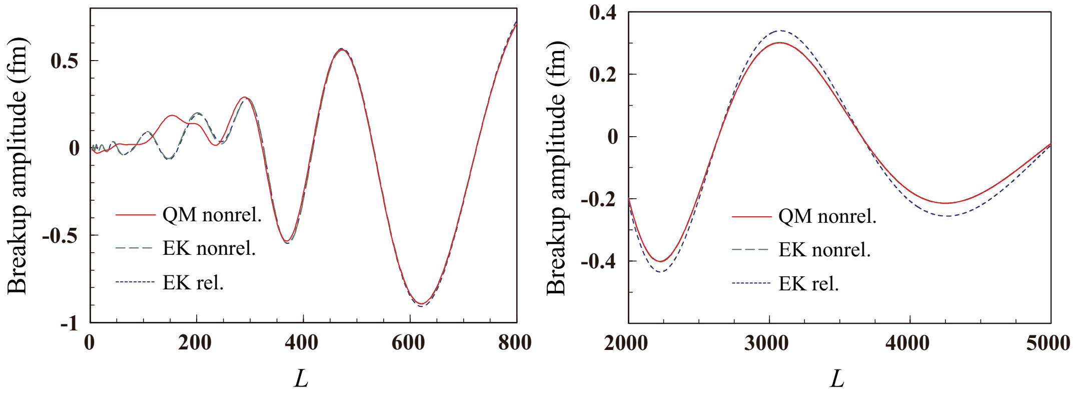

Fig. 8. Real part of breakup amplitude for ^{8}B+^{208}Pb at 250 MeV/nucleon as a function of the orbital angular momentum L between ^{8}B and ^{208}Pb. The final state of ^{8}B is chosen to be the s-wave 6th bin state, and the z-component m_0 of the spin of ^{8}B in the incident channel chosen as 1. The solid, dashed, and dotted lines show the results of nonrelativistic QM CDCC, nonrelativistic E-CDCC, and relativistic E-CDCC, respectively.

L and that by relativistic E-CDCC for large L allows one to construct an accurate coupled-channel framework that includes dynamical relativistic corrections and QM effects, i.e., *relativistic CDCC*.

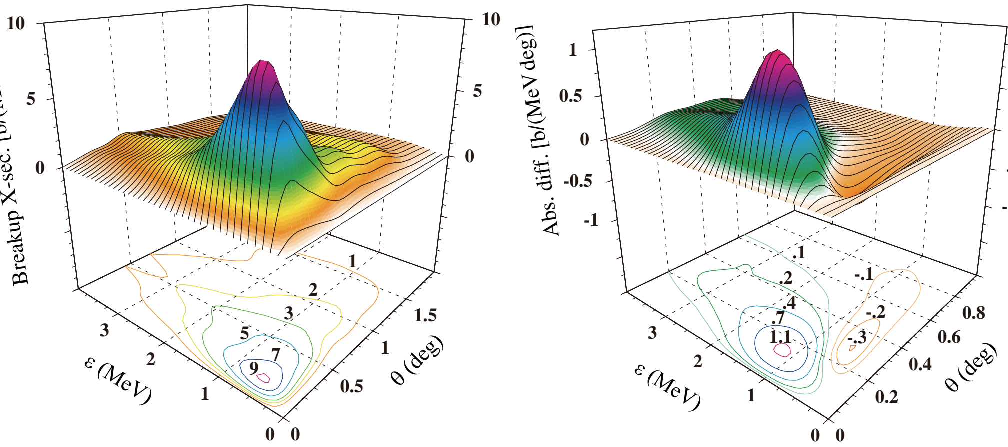

Fig. 9. Double differential breakup cross section (DDBUX) for ^{8}B+^{208}Pb at 250 MeV/nucleon including dynamical relativistic corrections (left panel), and its difference from the calculation without relativistic corrections (right panel).

In the left panel of Fig. 9 we show the double differential breakup cross section (DDBUX), $d^2\sigma_{\rm BU}/(d\epsilon d\theta)$, for the ^{8}B+^{208}Pb reaction at 250 MeV/nucleon calculated with relativistic CDCC based on Eq. (4·15). ϵ is the relative energy of the two fragments, p and ^{7}Be, of ^{8}B after the breakup, and θ is the scattering angle of the c.m. of ^{8}B (the p and ^{7}Be system). The right panel shows the difference of the DDBUX in the left panel from that calculated with nonrelativistic CDCC, which also is based on

Eq. (4·15) but including no dynamical relativistic corrections. Note that a relativistic treatment of the kinematics is adopted in both calculations. One observes a sizable increase in the DDBUX due to relativity at forward angles ($\theta \lesssim 0.2^\circ$) and around $\epsilon = 1$ MeV, where the DDBUX has quite large values as shown in the left panel. The increase is indeed large, i.e., several tens of %, which shows the importance of including dynamical relativistic corrections in analysis of Coulomb breakup at intermediate energies.

Thus, we have developed E-CDCC for treating both nuclear and Coulomb breakup very accurately and efficiently. The scattering amplitude f_{c0} to each channel c is expressed as a sum of the partial amplitudes $f'_{L;c0}$ with L the "classical" orbital angular momentum. The QM corrections in f_{c0} can be made by replacing the $f'_{L;c0}$ with the corresponding CDCC results, and the replacement is necessary only for small L. E-CDCC calculations with the QM corrections are much faster than CDCC calculations, with keeping the same accuracy as of the latter. In addition to that, E-CDCC makes it clear the relation between the eikonal picture and the QM picture. Furthermore, E-CDCC can incorporate a relativistic Liénard-Wiechert potential as a Coulomb interaction and the dynamical relativistic effects generated. E-CDCC has thus become a standard method for describing breakup reactions in which the Coulomb breakup contribution is essential.

§5. Proposal of four-body CDCC as a method of treating breakup of three-body projectile

In this section, we present a new version of CDCC to treat four-body breakup reactions, in which the projectile breaks up into three constituents, i.e., *four-body CDCC*. In principle, CDCC is a method of treating many-body reaction systems. However, except for three-body reactions that involve two-body projectiles, it is difficult to solve the CDCC equation. The main problem of the difficulty is how to calculate a set of discretized continuum states for a many-body projectile.

For the discretization procedure, as mentioned in §2, three methods have been proposed so far: the average (Av) method, the midpoint (Mid) method, and the pseudostate (PS) method. The Av method has been widely used and successful in describing three-body breakup reactions. The Mid method is shown to give the same results as of the Av method.[67),68)] These two methods are, however, difficult to apply to many-body reaction systems, where the projectile is to be described as at least a three-body system. The main difficulty lies on obtaining the discretized continuum states of such projectiles; both the Av method and the Mid method require the exact many-body continuum wave functions of projectile. An alternative to the Av and Mid methods is the PS method,[47),49),48),50),54),57)] in which the continuum states are replaced by pseudostates obtained by diagonalizing the internal Hamiltonian of the projectile in a space spanned by L^2-type basis functions. One can adopt the transformed harmonic oscillator (THO)[54)] or the Gaussian[47),49)] form as the basis functions. The validity of the PS method was confirmed for scattering of two-body projectiles by the agreement between CDCC solutions calculated with the Av and

PS methods.[47),49)]

A great advantage of the PS method is that we do not need exact continuum wave functions to obtain discretized continuum states, which is an essential point to extend CDCC for many-body reaction systems. CDCC with the PS method based on Gaussian basis functions was shown to be highly successful in describing the elastic scattering of ^{6}He, a typical three-body ($\alpha + n + n$) projectile, at not only high energies but also low energies near the Coulomb barrier;[48),50)] see §7.3 for the details. Thus, we have developed a new framework, *four-body CDCC*, for describing a reaction process of a three-body projectile and a target nucleus, explicitly taking account of breakup channels of the four-body reaction system. Later, a four-body CDCC calculation with the THO basis was also successfully carried out for low energy ^{6}He elastic scattering.[57)]

There is another difficulty in describing many-body breakup reactions, i.e., how to obtain a smooth breakup cross section with respect to the breakup energy ε of the many-body system. Because of the discretization of the continuum states of the projectile, solving CDCC equations provides breakup S-matrix elements to the discretized-continuum states, which give discrete breakup cross sections. On the other hand, the breakup cross section in reality is of course continuous as a function of ε. Thus, one needs a way of smoothing the discretized breakup S-matrix elements.

If we could adopt the Av method, the smoothing procedure was straightforward, because of the clear relation between the continuum state and the discretized continuum one. In fact, there has been an attempt[59)] to apply the Av method to ^{6}He breakup processes by directly calculating the three-body continuum state with utilizing the hyperradial continuum wave functions.[111)] Though this alternative four-body CDCC worked very well for the elastic scattering of ^{6}He, convergence of the breakup cross section $d\sigma/d\varepsilon$ was not obtained as indicated in Fig. 5 of Ref. 59).

With the PS discretization, we can smooth the breakup cross section by calculating the smoothing function $\langle \psi^{(-)}(\varepsilon)|\Phi_\gamma\rangle$, where $\psi^{(-)}(\varepsilon)$ is the exact continuum wave function with the incoming boundary condition and Φ_γ is the γth discretized continuum state. Details of this smoothing procedure are shown in Refs. 47) and 52) for three-body reactions and in Ref. 51) for four-body reactions. This method is much more practical than the aforementioned Av method for the three-body projectile, because we need only the overlap of $\psi^{(-)}(\varepsilon)$ with the spatially damping (compact) wave function Φ_γ. To obtain a convergence of $d\sigma/d\varepsilon$ with very high accuracy is, however, still difficult at present.

In this situation, very recently, we proposed a new smoothing procedure[53)] with the complex-scaling method.[112)] The advantage of this method is that we do not need the exact continuum wave function at all, i.e., only the overlap between two compact wave functions is required. Below we describe this new method for the scattering of ^{6}He by a target A, as a typical example of four-body reactions.

The Schrödinger equation for the four-body system of our interest is given by

$$[H - E_{\rm tot}]|\Psi^{(+)}\rangle = 0, \tag{5·1}$$

where (+) indicates the outgoing boundary condition and $E_{\rm tot}$ is the total energy of the system. The total Hamiltonian H is defined by

$$H = K_R + h_{\rm P} + U_{n{\rm A}} + U_{n{\rm A}} + U_{\alpha{\rm A}}, \qquad (5\cdot2)$$

where the internal Hamiltonian $h_{\rm P}$ of ^{6}He is given by

$$h_{\rm P} = K_y + K_r + V_{nn} + V_{n\alpha} + V_{n\alpha} \qquad (5\cdot3)$$

within the $\alpha + n + n$ three-body model adopted. The relative coordinate between ^{6}He and A is denoted by $\boldsymbol{R}$ and the internal coordinates of ^{6}He by a set of Jacobi coordinates, $\boldsymbol{\xi} = (\boldsymbol{y}, \boldsymbol{r})$. The kinetic energy operator associated with $\boldsymbol{R}$ ($\boldsymbol{\xi}$) is represented by K_R (K_ξ), $V_{xx'}$ is a nuclear interaction between x and x', and $U_{x{\rm A}}$ is the sum of the nuclear and Coulomb potentials between x and A.

In CDCC with the PS method, the reaction process is assumed to take place in a model space

$$\mathcal{P}' = \sum_\gamma |\Phi_\gamma\rangle\langle\Phi_\gamma|, \qquad (5\cdot4)$$

where the Φ_γ are the eigenstates obtained by diagonalizing $h_{\rm P}$ by L^2-type basis functions. Details of the calculation for Φ_γ are shown later in this section. The four-body Schrödinger equation is then solved in the model space

$$\mathcal{P}'[H - E_{\rm tot}]\mathcal{P}'|\Psi^{(+)}_{\rm CDCC}\rangle = 0. \qquad (5\cdot5)$$

This so-called model space assumption has already been justified as mentioned in §2; there is no essential difference between three-body CDCC and four-body CDCC in this point. In fact, we have confirmed that elastic and breakup cross sections calculated with three-body CDCC or four-body CDCC converged with respect to expanding the model space.[47),49),48),50)]

The exact T-matrix element to a breakup state of the $\alpha + n + n$ system is given by

$$T_\varepsilon(\boldsymbol{p}, \boldsymbol{k}, \boldsymbol{P}) = \langle\psi^{(-)}_\varepsilon(\boldsymbol{p}, \boldsymbol{k})\chi^{(-)}_\varepsilon(\boldsymbol{P})|U - U^{\rm (Coul)}_{^6{\rm He}}|\Psi^{(+)}\rangle, \qquad (5\cdot6)$$

where $U = U_{n{\rm A}} + U_{n{\rm A}} + U_{\alpha{\rm A}}$ and $U^{\rm (Coul)}_{^6{\rm He}}$ is the Coulomb interaction between ^{6}He and A. $\boldsymbol{P}$, $\boldsymbol{p}$, and $\boldsymbol{k}$ are the asymptotic relative momenta conjugate to the coordinate $\boldsymbol{R}$, $\boldsymbol{y}$, and $\boldsymbol{r}$, respectively. These three momenta specify the kinematics of the four particles to be detected in measurements. The final-state wave functions, $|\psi^{(-)}_\varepsilon(\boldsymbol{p}, \boldsymbol{k})\rangle$ and $|\chi^{(-)}_\varepsilon(\boldsymbol{P})\rangle$, with the incoming boundary condition, are defined by

$$\left[T_R + U^{\rm (Coul)}_{^6{\rm He}} - (E_{\rm tot} - \varepsilon)\right]|\chi^{(-)}_\varepsilon(\boldsymbol{P})\rangle = 0, \qquad (5\cdot7)$$

$$[h_{\rm P} - \varepsilon]\,|\psi^{(-)}_\varepsilon(\boldsymbol{p}, \boldsymbol{k})\rangle = 0, \qquad (5\cdot8)$$

where $E_{\rm tot} - \varepsilon = (\hbar P)^2/(2\mu_R)$ and $\varepsilon = (\hbar p)^2/(2\mu_y) + (\hbar k)^2/(2\mu_r)$; the μ are the reduced masses regarding the relative coordinate given in the subscript. Inserting the approximate complete set Eq. (5·4) into Eq. (5·6), one can get with high accuracy the T-matrix element[47]

$$T_\varepsilon(\boldsymbol{p},\boldsymbol{k},\boldsymbol{P}) \approx \sum_{\gamma\neq 0}\langle\psi_\varepsilon^{(-)}(\boldsymbol{p},\boldsymbol{k})|\varPhi_\gamma\rangle T_\gamma \tag{5·9}$$

with the CDCC T-matrix element

$$T_\gamma = \langle\varPhi_\gamma\chi_{\varepsilon_\gamma}^{(-)}(\boldsymbol{P}_\gamma)|U - U_{^6\mathrm{He}}^{(\mathrm{Coul})}|\varPsi_{\mathrm{CDCC}}^{(+)}\rangle \tag{5·10}$$

to the γth discrete breakup state $\varPhi_\gamma$ that has the eigenenergy ε_γ. Equation (5·9) has been derived by replacing $\boldsymbol{P}$ with $\boldsymbol{P}_\gamma$ in $\chi_\varepsilon^{(-)}(\boldsymbol{P})$. The T_γ are obtainable by CDCC, but it is quite hard to calculate the smoothing function $\langle\psi_\varepsilon^{(-)}(\boldsymbol{p},\boldsymbol{k})|\varPhi_\gamma\rangle$ directly as mentioned above. Fortunately, however, one can find a way of circumventing this difficulty for the calculation of the double differential breakup cross section (DDBUX) $d^2\sigma/(d\varepsilon d\varOmega_{\boldsymbol{P}})$.

Using Eq. (5·9), one can rewrite the DDBUX as

$$\frac{d^2\sigma}{d\varepsilon d\varOmega_{\boldsymbol{P}}} = \frac{(2\pi)^4\mu_R^2}{\hbar^4}\frac{P}{P_0}\int d\boldsymbol{p}'d\boldsymbol{k}'\delta(\varepsilon-\varepsilon')|T_{\varepsilon'}(\boldsymbol{p}',\boldsymbol{k}',\boldsymbol{P}')|^2 \approx \frac{1}{\pi}\mathcal{R}(\varepsilon,\varOmega_{\boldsymbol{P}}) \tag{5·11}$$

with the generalized response function

$$\mathcal{R}(\varepsilon,\varOmega_{\boldsymbol{P}}) = \frac{(2\pi)^4\mu_R^2}{\hbar^4}\frac{P}{P_0}\mathrm{Im}\Big[\sum_{\gamma,\gamma'\neq 0} T_\gamma^*\langle\varPhi_\gamma|G^{(-)}|\varPhi_{\gamma'}\rangle T_{\gamma'}\Big], \tag{5·12}$$

where $G^{(-)}$ is the propagator given by

$$G^{(-)} = \lim_{\eta\to+0}\frac{1}{\varepsilon - h_{\mathrm{P}} - i\eta}. \tag{5·13}$$

The propagator $G^{(-)}$ operates only on spatially damping functions $\varPhi_\gamma$. This makes the calculation of $\langle\varPhi_\gamma|G^{(-)}|\varPhi_{\gamma'}\rangle$ feasible.

We now use the complex-scaling method in which the scaling transformation operator $C(\theta)$ and its inverse are defined by

$$\langle\boldsymbol{r},\boldsymbol{y}|C(\theta)|f\rangle = e^{3i\theta}f(\boldsymbol{r}e^{i\theta},\boldsymbol{y}e^{i\theta}), \tag{5·14}$$

$$\langle f|C^{-1}(\theta)|\boldsymbol{r},\boldsymbol{y}\rangle = \{e^{-3i\theta}f(\boldsymbol{r}e^{-i\theta},\boldsymbol{y}e^{-i\theta})\}^*. \tag{5·15}$$

Using these operators, one can get

$$\langle\varPhi_\gamma|G^{(-)}|\varPhi_{\gamma'}\rangle = \langle\varPhi_\gamma|C^{-1}(\theta)G_\theta^{(-)}C(\theta)|\varPhi_{\gamma'}\rangle, \tag{5·16}$$

where

$$G_\theta^{(-)} = \lim_{\eta\to+0}\frac{1}{\varepsilon - h_{\mathrm{P}}^\theta - i\eta} \tag{5·17}$$

with $h_{\mathrm{P}}^\theta = C(\theta)h_{\mathrm{P}}C^{-1}(\theta)$. When $-\pi < \theta < 0$, the scaled propagator $\langle\boldsymbol{\xi}|G_\theta^{(-)}|\boldsymbol{\xi}'\rangle$ is a damping function of $\boldsymbol{\xi}$ and $\boldsymbol{\xi}'$. Note that positive θ has been taken so far in the complex-scaling method, but in the present situation it must be negative since $G^{(-)}$ has the incoming boundary condition. The scaled propagator $G_{\theta}^{(-)}$ is a L^2-type function,[52)] and is then expanded with L^2-type basis functions:

$$G_{\theta}^{(-)} \approx \sum_{i} \frac{|\phi_i^{\theta}\rangle\langle\tilde{\phi}_i^{\theta}|}{\varepsilon - \varepsilon_i^{\theta}}, \tag{5·18}$$

where ϕ_i^{θ} is the ith eigenstate of $h_{\rm P}^{\theta}$ in a model space spanned by L^2-type basis functions, i.e., $\langle\tilde{\phi}_i^{\theta}|h_{\rm P}^{\theta}|\phi_{i'}^{\theta}\rangle = \varepsilon_i^{\theta}\delta_{ii'}$. Inserting Eq. (5·16) with Eq. (5·18) into Eq. (5·12) leads to a desired form

$$\frac{d^2\sigma}{d\varepsilon d\Omega_{\boldsymbol{P}}} \approx \frac{1}{\pi}\frac{(2\pi)^4\mu_R^2}{\hbar^4}\frac{P}{P_0}{\rm Im}\sum_{i}\frac{T_i^{\theta}\tilde{T}_i^{\theta}}{\varepsilon - \varepsilon_i^{\theta}} \tag{5·19}$$

with

$$\tilde{T}_i^{\theta} \equiv \sum_{\gamma'}\langle\tilde{\phi}_i^{\theta}|C(\theta)|\Phi_{\gamma'}\rangle T_{\gamma'}, \quad T_i^{\theta} \equiv \sum_{\gamma} T_{\gamma}^{*}\langle\Phi_{\gamma}|C^{-1}(\theta)|\phi_i^{\theta}\rangle. \tag{5·20}$$

Equation (5·19) contains no exact three-body continuum states $\psi_{\varepsilon}^{(-)}(\boldsymbol{k},\boldsymbol{p})$. This is the most important advantage of this new smoothing procedure.

It should be noted that the use of the response function in the complex-scaling method to obtain smooth breakup spectra has already been done in some previous studies.[113),114)] The essential feature of the present study is the extension of the method for genuine reaction calculations. As mentioned above, the T-matrix element T_{γ} in Eq. (5·20) is the solution of the CDCC calculation for the scattering of a many-body projectile by a target nucleus, which thus contains all degrees of freedom of reaction dynamics within the model space adopted.

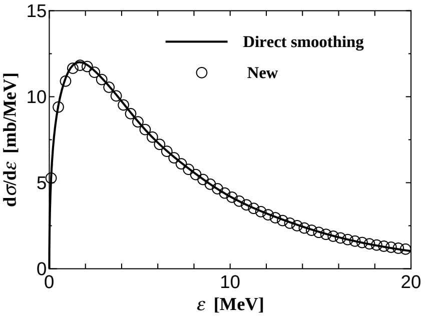

Fig. 10. Breakup cross section for the d+^{58}Ni scattering at 80 MeV. The solid line is the result of the direct smoothing method and the open circles show the result of the new method.

We tested first the validity of Eq. (5·19) for a three-body breakup reaction, for which the exact breakup T-matrix element $T(\boldsymbol{k},\boldsymbol{P}) = \sum_n\langle\psi^{(-)}(\boldsymbol{k})|\Phi_n\rangle T_n$ is obtainable by taking the overlap $\langle\psi^{(-)}(\boldsymbol{k})|\Phi_n\rangle$ directly.[47)] This approach is referred to as *the direct smoothing method* below. As an example, we consider the ^{58}Ni(d, pn) reaction at 80 MeV; see Ref. 47) for the details of the CDCC calculation. Figure 10 shows the differential breakup cross section $d\sigma/d\varepsilon$, which is obtained by integrating the DDBUX of Eq. (5·19) over the solid angle $\Omega_{\boldsymbol{P}}$. The new method (open circles) yields the same result as the direct smoothing method (solid line). The validity of the new method is thus confirmed.

Next, the new method is applied to the ^{12}C(^{6}He, αnn) reaction at 229.8 MeV. As for the interactions V_{nn} and $V_{n\alpha}$ in $h_{\rm P}$, we take the GPT[115)] and KKNN[116)] potentials, respectively. These potentials with a Gaussian form reproduce well experimental data of low-energy nucleon-nucleon and nucleon-α scattering. The particle exchange between valence neutrons and neutrons in α is treated approximately with the orthogonality condition model.[117)]

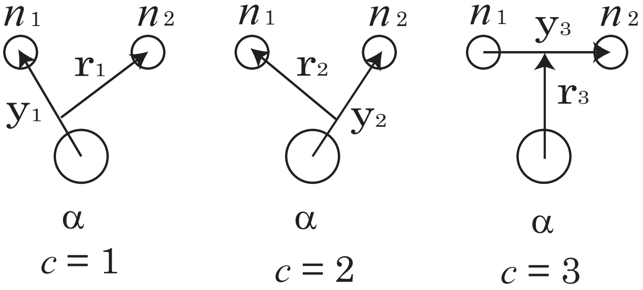

Fig. 11. Jacobi coordinates of three rearrangement channels (c = 1–3) of ^{6}He.

For the diagonalization of $h_{\rm P}$ and $h_{\rm P}^{\theta}$, we adopt the Gaussian expansion method (GEM).[118)] In GEM, the $\alpha + n + n$ system is described by a superposition of three channels, each of which corresponds to a different set of Jacobi coordinates $(\boldsymbol{y}_c, \boldsymbol{r}_c)$, as shown in Fig. 11. For each channel (c), the radial parts of the internal wave functions are expanded by a finite number of Gaussian basis functions

$$\varphi_{j\lambda}(\boldsymbol{y}_c) = y_c^{\lambda} e^{-(y_c/\bar{y}_j)^2} Y_\lambda(\Omega_{y_c}), \quad \varphi_{i\ell}(\boldsymbol{r}_c) = r_c^{\ell} e^{-(r_c/\bar{r}_i)^2} Y_\ell(\Omega_{r_c}), \tag{5·21}$$

where λ (ℓ) is the orbital angular momentum regarding $\boldsymbol{y}_c$ ($\boldsymbol{r}_c$). The range parameters $\bar{y}_j$ and $\bar{r}_i$ are taken to lie in geometric progression

$$\bar{y}_j = (\bar{y}_{\rm max}/\bar{y}_1)^{(j-1)/j_{\rm max}}, \quad \bar{r}_i = (\bar{r}_{\rm max}/\bar{r}_1)^{(i-1)/i_{\rm max}}. \tag{5·22}$$

The parameters actually depend on c, but we omitted the dependence in Eq. (5·22) for simplicity. In order to confirm the convergence of the breakup cross section with

Table I. Gaussian range parameters.

Set	c	$j_{\rm max}$	$\bar{y}_1$ (fm)	$\bar{y}_{\rm max}$ (fm)	$i_{\rm max}$	$\bar{r}_1$ (fm)	$\bar{r}_{\rm max}$ (fm)
I	3	10	0.1	10.0	10	0.5	10.0
	1, 2	10	0.5	10.0	10	0.5	10.0
II	3	15	0.1	20.0	15	0.5	20.0
	1, 2	15	0.5	20.0	15	0.5	20.0
III	3	20	0.1	50.0	20	0.5	50.0
	1, 2	20	0.5	50.0	20	0.5	50.0

respect to the size of the model space, we prepare the three sets of basis functions shown in Table I. For the 0^+ and 1^- states, maximum internal angular momenta $\ell_{\rm max}$ and $\lambda_{\rm max}$ are both set to unity. For the 2^+ states, we take $\ell_{\rm max} = \lambda_{\rm max} = 1$ for $c = 1$ and 2, and $\ell_{\rm max} = \lambda_{\rm max} = 2$ for $c = 3$. For other numerical inputs, see Ref. 53).

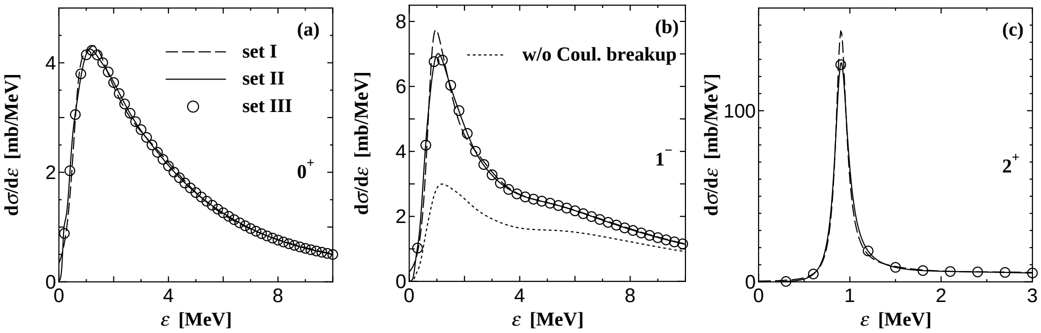

Fig. 12. Convergence of the breakup cross sections to the 0^+ (a), 1^- (b), and 2^+ (c) continua. In each panel, the dashed line, the solid line, and the open circles correspond to results of sets I, II, and III, respectively. The dotted line in (b) shows the result when Coulomb breakup processes are switched off.

Figure 12 shows the breakup cross sections $d\sigma/d\varepsilon$ to the 0^+, 1^-, and 2^+ continua. For all the cross sections, sets II and III yield the same result, whereas the result of set I is somewhat different from it. The convergence of CDCC solution with respect to expanding the model space is thus obtained with set II. Figure 13 shows the breakup cross sections for four values of the complex-scaling angle θ. All the breakup cross sections converge at $\theta = -14^\circ$, when θ decreases from -6° to -18°.

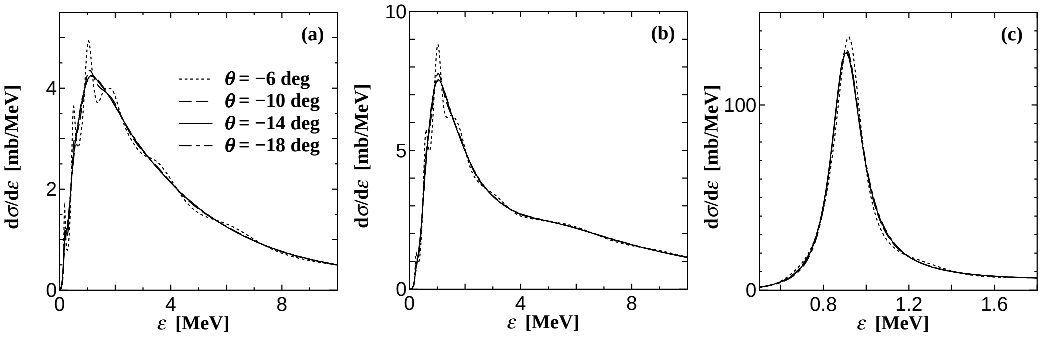

Fig. 13. Dependence of the breakup cross section to the 0^+ (a), 1^- (b), and 2^+ (c) continua on complex-scaling angle θ.

The present calculation includes nuclear and Coulomb breakup processes. The contribution of the latter is indeed large for the breakup to the 1^- continuum, as indicated by the dotted line in Fig. 12(b). It increases the breakup cross section by a factor of 2 from the result without Coulomb breakup. On the other hand, the Coulomb breakup effect turns out to be negligible for the 0^+ and 2^+ breakup spectra, and the latter dominates the breakup cross section. Consequently, the

Coulomb breakup effect in the present reaction system is not significant for both the breakup reaction and the elastic scattering. For heavier targets, however, Coulomb breakup processes become dominant. Four-body CDCC can treat both nuclear and Coulomb breakup processes and hence their interference. In §7.3, we apply four-body CDCC to ^{6}He scattering from both light and heavy targets in a wide range of incident energies.

§6. Proposal of the eikonal reaction theory (ERT) that makes CDCC applicable to inclusive reactions

CDCC is highly reliable for describing exclusive reactions but not applicable to inclusive cross sections such as a neutron removal cross section. In this section, we present an accurate method of treating inclusive reactions within the framework of CDCC. According to the method, the nuclear and Coulomb breakup processes are consistently treated by CDCC without making the adiabatic approximation to the Coulomb interaction, so that the removal cross section calculated never diverges. This method is referred to as *the eikonal reaction theory (ERT).* This section consists of a brief review of Refs. 119) and 120), and a new application of ERT to two-neutron removal reactions.

6.1. *Formulation of ERT*

Let us consider as a projectile (P) the two-body system composed of a core nucleus (c) and a valence neutron (n), and hence the three-body (c+n+A) system for the scattering of P from a target A. We start with the S-matrix operator as a formal solution to the coupled-channel (E-CDCC) equations (4·5) in §4,

$$S = \exp\Big[-i\mathcal{C}\int_{-\infty}^{\infty} dz \hat{O}^{\dagger} U \hat{O}\Big] \tag{6·1}$$

with the interaction

$$U = U_n^{(\mathrm{Nucl})} + U_{\mathrm{c}}^{(\mathrm{Nucl})} + U_{\mathrm{c}}^{(\mathrm{Coul})}, \tag{6·2}$$

where $U_n^{(\mathrm{Nucl})}$ is the nuclear part of the optical potential between n and A, and $U_{\mathrm{c}}^{(\mathrm{Nucl})}$ and $U_{\mathrm{c}}^{(\mathrm{Coul})}$ are, respectively, the nuclear and Coulomb parts of the optical potential between c and A. $\mathcal{C}$ is the path ordering operator which describes the multistep scattering processes accurately. The operator $\hat{O}$ is defined by

$$\hat{O} = \frac{1}{\sqrt{\hbar\hat{v}}} e^{i\hat{K}\cdot z}, \tag{6·3}$$

where the wave-number operator $\hat{K}$ is given by $\hat{K} = \sqrt{2\mu_R(E-h)}/\hbar$ with the internal Hamiltonian h of P, and $\hat{v} = \hbar\hat{K}/\mu_R$ is the velocity operator. In the definition of $\hat{O}$ we assume that there is no Coulomb monopole interaction between P and A for simplicity. In the actual calculation, the exponent in Eq. (4·2), with K_c and η_c replaced with the operator form, is used as an exponent in $\hat{O}$; the form of $\hat{v}$ is changed accordingly.

In the Glauber model, the adiabatic approximation is made, in which h is replaced with the ground-state energy ϵ_0, and hence $\hat{O}^\dagger U \hat{O}$ and $\mathcal{C}$ in Eq. (6·1) are reduced to $U/(\hbar v_0)$ and 1, respectively, where v_0 is the velocity of P in the ground state relative to A. At intermediate energies, this treatment is known to be valid for short-range nuclear interactions, but not for the long-range Coulomb interactions. Therefore, we make the adiabatic approximation in the evaluation of only $\hat{O}^\dagger U_n^{(\mathrm{Nucl})} \hat{O}$, i.e., we use

$$\hat{O}^\dagger U_n^{(\mathrm{Nucl})} \hat{O} \to U_n^{(\mathrm{Nucl})}/(\hbar v_0). \tag{6·4}$$

For the scattering of ^{31}Ne from a ^{208}Pb target at 240 MeV/nucleon, it is shown by CDCC that the effect due to the replacement (6·4) is small; it is 0.2% for the reaction cross section σ_{R}, 1.9% for the elastic-breakup cross section σ_{EB}, 4.1% for the one-neutron stripping cross section $\sigma_{n:\mathrm{STR}}$. Using this replacement, S can be separated into the neutron part S_n and the core part S_{c},

$$S = S_n S_{\mathrm{c}} \tag{6·5}$$

with

$$S_n = \exp\Big[-\frac{i}{\hbar v_0}\int_{-\infty}^{\infty} dz U_n^{(\mathrm{Nucl})}\Big], \tag{6·6}$$

$$S_{\mathrm{c}} = \exp\Big[-i\mathcal{C}\int_{-\infty}^{\infty} dz \hat{O}^\dagger (U_{\mathrm{c}}^{(\mathrm{Nucl})} + U_{\mathrm{c}}^{(\mathrm{Coul})})\hat{O}\Big]. \tag{6·7}$$

This is the most important result of ERT. We can derive several kinds of cross sections with the product form Eq. (6·5), following the formulation of the cross sections in the Glauber model;16),17) see, e.g., Ref. 120) for the explicit form of them. It should be noted that one cannot evaluate S_{c} directly with Eq. (6·7), since it includes the operators $\hat{O}$ and $\mathcal{C}$. However, one may find that S_{c} is the formal solution to the Schrödinger equation

$$\Big[-\frac{\hbar^2}{2\mu_R}\nabla_R^2 + h + U_{\mathrm{c}}^{(\mathrm{Nucl})} + U_{\mathrm{c}}^{(\mathrm{Coul})} - E\Big]\Psi_{\mathrm{c}} = 0, \tag{6·8}$$

when the eikonal approximation is made. We can thus obtain S_{c} by solving Eq. (6·8) with E-CDCC.45),46) As mentioned above, S_n is obtained by Eq. (6·6).

6.2. *One-neutron removal reaction of ^{31}Ne*

We apply ERT to the one-neutron removal reactions for the ^{31}Ne+^{12}C scattering at 230 MeV/nucleon and the ^{31}Ne+^{208}Pb scattering at 234 MeV/nucleon with a ^{30}Ne+n+A three-body model. The optical potentials for the n-target and ^{30}Ne-target subsystems are obtained by folding the effective nucleon-nucleon interaction121) with one-body nuclear densities. The densities of P and A are constructed by the same method as in Ref. 122). We assume the ground state of ^{31}Ne to be either the ^{30}Ne$(0^+) \otimes$ 1p3/2 or the ^{30}Ne$(0^+) \otimes$ 0f7/2, with the one-neutron separation energy of 0.33 MeV. As for the breakup states, we include s-, p-, d-, f-, and g-waves up to the relative momentum between ^{30}Ne and n of 0.8 fm^{-1}. For more detailed numerical inputs, see Ref. 119).

Table II presents the integrated elastic-breakup cross section $\sigma_{\rm EB}$, the one-neutron stripping cross section $\sigma_{n:{\rm STR}}$, the one-neutron removal cross section σ_{-n}, and the spectroscopic factor $\mathcal{S} = \sigma_{-n}^{\rm exp}/\sigma_{-n}^{\rm th}$. $\mathcal{S}$ calculated with the 1p3/2 ground-state neutron configuration little depends on the target and less than unity, but that with the 0f7/2 configuration does not satisfy these conditions. Therefore, we can infer that the major component of the ground state of ^{31}Ne is $^{30}{\rm Ne}(0^+)\otimes 1{\rm p}3/2$ with $\mathcal{S} \sim 0.69$. This value is consistent with the result shown in Sec. 3.5. We adopt this configuration in the following.

Table II. Integrated cross sections and the spectroscopic factor for the ^{31}Ne-^{12}C scattering at 230 MeV/nucleon and the ^{31}Ne-^{208}Pb scattering at 234 MeV/nucleon. The cross sections are presented in unit of mb and the data are taken from Ref. 12).

	^{12}C target			^{208}Pb target		
	$\rm p_{3/2}$	$\rm f_{7/2}$	Exp.	$\rm p_{3/2}$	$\rm f_{7/2}$	Exp.
$\sigma_{\rm EB}$	23.3	3.3		799.5	73.0	(540)
$\sigma_{n:{\rm STR}}$	90	29		244	53	
σ_{-n}	114	32	79	1044	126	712
$\mathcal{S}$	0.693	2.47		0.682	5.65	

Since the potential between ^{30}Ne and n is not well known, we change each of the potential parameters by 30% and see how this ambiguity of the potential affects the resulting value of $\mathcal{S}$. We obtain $\mathcal{S} = 0.693 \pm 0.133 \pm 0.061$ for a ^{12}C target and $\mathcal{S} = 0.682 \pm 0.133 \pm 0.062$ for a ^{208}Pb target; the second and third numbers following the mean value stand for the theoretical and experimental uncertainties, respectively. Thus, $\mathcal{S}$ includes a sizable theoretical uncertainty. This situation completely changes if we look at the asymptotic normalization coefficient C,[123)] i.e., $C = 0.320 \pm 0.010 \pm 0.028$ fm$^{-1/2}$ for a ^{12}C target and $C = 0.318 \pm 0.008 \pm 0.029$ fm$^{-1/2}$ for a ^{208}Pb target. Thus, C has a much smaller theoretical uncertainty than $\mathcal{S}$. This means that the one-nucleon removal reaction is quite peripheral.

6.3. *Two-neutron removal reaction of ^{6}He*

ERT is applied to two-neutron removal reactions of ^{6}He from ^{12}C and ^{208}Pb targets at 240 MeV/nucleon. In this case, the projectile is treated as a three-body ($\alpha+n+n$) system and hence four-body CDCC is used. The optical potentials for the n-target and α-target subsystems are calculated by folding the Melbourne nucleon-nucleon g-matrix interaction[79)] with the densities obtained by the spherical Hartree-Fock (HF) calculation with the Gogny D1S interaction.[99),100)] The model space of the following calculation is the same as in Ref. 53), with which good convergence is achieved.

Table III shows the one- and two-neutron stripping cross sections, $\sigma_{n:{\rm STR}}$ and $\sigma_{2n:{\rm STR}}$, respectively, and the two-neutron removal cross section σ_{-2n}. The present framework reproduces well the experimental data[124)] with no adjustable parameters. Thus, we can clearly see the reliability of ERT for two-neutron removal reactions on both light and heavy targets.

Table III. Integrated cross sections for two-neutron removal reaction of ^{6}He on ^{12}C and ^{208}Pb targets at 240 MeV/nucleon. The cross sections are presented in unit of mb and the experimental data are taken from Ref. 124).

	^{12}C target		^{208}Pb target	
	Calc.	Exp.	Calc.	Exp.
$\sigma_{n:\mathrm{STR}}$	153.4	127 ± 14	353.6	320 ± 90
$\sigma_{2n:\mathrm{STR}}$	29.0	33 ± 23	148.9	180 ± 100
σ_{-2n}	198.5	190 ± 18	1016.6	1150 ± 90

6.4. *Comparison of ERT and the Glauber model*

In this subsection, the accuracy of the Glauber model is tested for deuteron induced reactions at 200 MeV/nucleon. We estimate the relative difference

$$\delta_X = [X(\mathrm{CDCC}) - X(\mathrm{GL})]/X(\mathrm{CDCC}), \qquad (6{\cdot}9)$$

where $X(\mathrm{CDCC})$ and $X(\mathrm{GL})$ correspond to integrated cross sections calculated by CDCC with ERT and the Glauber model, respectively. For the Glauber-model calculation in which the eikonal and adiabatic approximations are made, the Coulomb interaction is neglected. The numerical inputs are given in Ref. 120).

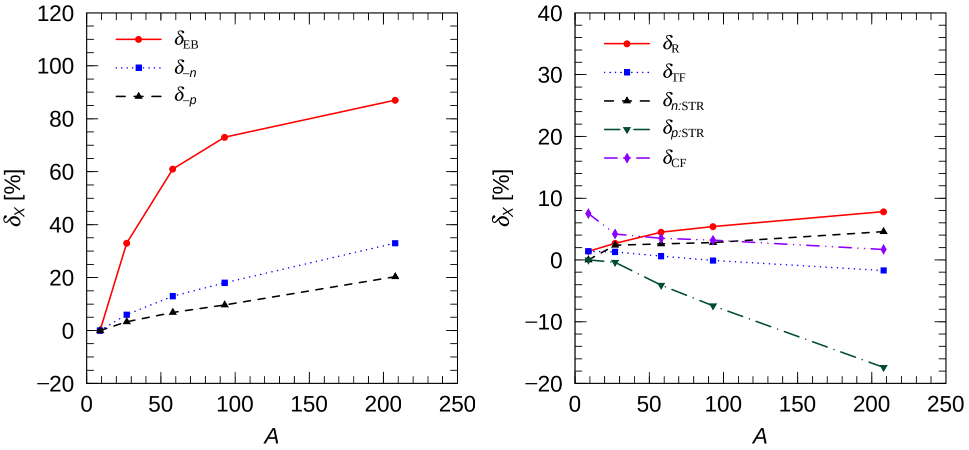

Fig. 14. Accuracy of the Glauber model for various integrated cross sections.

Figure 14 shows δ_X as a function of target mass number A for σ_{EB}, σ_{R}, $\sigma_{n:\mathrm{STR}}$, σ_{-n}, the proton stripping ($\sigma_{p:\mathrm{STR}}$) and removal (σ_{-p}) cross sections, the total fusion cross section σ_{TF}, and the complete fusion cross section σ_{CF}. The Glauber model is good for light targets, as expected. For heavier targets where the Coulomb breakup is essential, however, the Glauber model is not good for the elastic-breakup and proton stripping cross sections.

§7. Applications of CDCC to scattering of unstable nuclei

In this section, we review some recent applications of CDCC to scattering of unstable nuclei. See the references cited in the following subsections for the details of the formalism, numerical inputs, other results, and further discussion.

7.1. *One-neutron removal reactions of ^{18}C and ^{19}C on proton target*

One-neutron removal reactions have played a key role in investigating exotic properties of neutron-rich nuclei. For light targets such as Be and C, the so-called stripping model[125),126)] based on the eikonal approximation has been successful in describing the removal process. On the other hand, for a proton target, the removal process can be interpreted as an elastic breakup, since there is no excited state in the target, and also a neutron transfer process producing deuteron hardly occurs. Therefore, we should treat accurately the elastic breakup process for the one-neutron removal reactions on a proton target, to which the stripping model is not applicable.

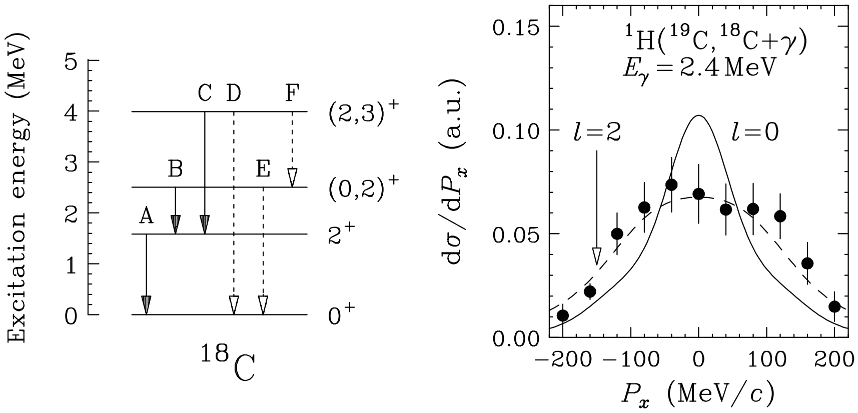

Fig. 15. Level scheme and transitions of ^{18}C (left panel) and transverse-momentum distribution of ^{18}C in coincidence with the 2.4 MeV γ-ray (right panel). The solid and dashed lines represent the CDCC calculations by assuming neutron removal from the $\ell = 0$ and $\ell = 2$ orbits in ^{19}C, respectively.

In Ref. 127), one neutron removal cross sections of ^{18}C and ^{19}C on a proton target were measured, and CDCC was applied to analyze the data to determine the neutron configuration of these nuclei. Figure 15 (right panel) shows the transverse-momentum distribution of ^{18}C after the breakup of ^{19}C in coincidence with the 2.4 MeV γ-ray, which corresponds to the population of the 4.0 MeV state of ^{18}C; see the level scheme in the left panel of Fig. 15. The experimental data are consistent with the CDCC calculation for neutron breakup from the 0d orbit in ^{19}C(1/2$^+$). From this analysis, we have successfully confirmed the spin-parity $I^\pi = (2,3)^+$ assignment for the 4.0 MeV state in ^{18}C; see Ref. 127) for more detailed discussion.

For both reactions induced by ^{18}C and ^{19}C, the theoretical cross sections calculated by CDCC with the shell-model spectroscopic factors obtained by the WBP interaction[128)] explain the most of the relative values, as shown in the Tables of Ref. 127). As for the absolute values, the measured and calculated results agree very well with each other for the breakup of ^{19}C that has a small neutron separation energy S_n. On the other hand, the measured cross section is significantly smaller than the calculated one for the breakup of ^{18}C that has a quite large S_n. This is consistent with the finding of a systematic analysis of nucleon removal cross sections,[10)] though the mechanism of this “quenching” of the shell-model spectroscopic factors is still under discussion. Thus, CDCC is shown to be a powerful method for determining configurations of valence neutrons in exotic nuclei.

7.2. *Study on the low-lying states in the unbound nucleus ^{13}Be*

Shell evolution of neutron-rich nuclei is one of the hottest topics of nuclear physics. In Ref. 129), we investigated the shell structure of ^{13}Be, which is unbound and has a neutron number $N = 9$. We did the same analysis as in §7.1 of the one-neutron removal cross section of ^{14}Be by a proton target.

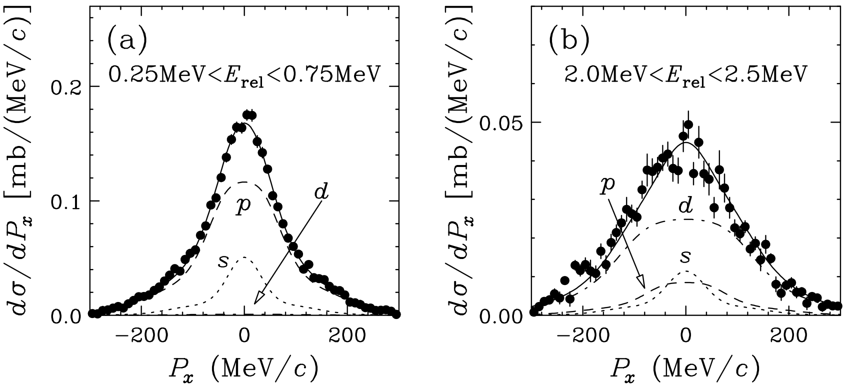

Fig. 16. Transverse momentum distributions of the ^{12}Be+n system for (a) 0.25 MeV $< E_{\rm rel} <$ 0.75 MeV and (b) 2.0 MeV $< E_{\rm rel} <$ 2.5 MeV. The s-, p-, and d-wave components are shown by the dotted, dashed, and dash-dotted lines, respectively. The solid lines are the sums of the three components.

We show in Fig. 16 the transverse momentum distributions of the ^{12}Be+n system for 0.25 MeV< $E_{\rm rel}$ <0.75 MeV (left panel) and 2.0 MeV< $E_{\rm rel}$ <2.5 MeV (right panel), where $E_{\rm rel}$ is the relative energy of ^{12}Be and n. The dotted, dashed, and dash-dotted lines correspond to the s-, p-, and d-wave contributions calculated by CDCC, respectively. We adopted a ^{13}Be+n two-body model with each of these relative angular momenta as an initial state structure of ^{14}Be, and then added all the results incoherently. The strengths of the individual components as well as the resonance parameters assumed were treated as free adjustable parameters to reproduce the experimental data; see Ref. 129) for more details. From this analysis, we confirmed the low-lying p-wave resonance at $E_{\rm rel} = 0.51(1)$ MeV as well as the d-wave resonance at $E_{\rm rel} = 2.39(5)$ MeV on the broad s-wave distribution with the s-wave scattering length $a_{\rm s} = -3.4(6)$ fm in the invariant mass spectrum of ^{13}Be. The spin-parity of the p-wave resonance state was assigned to $I^{\pi} = 1/2^-$. This intruder $1/2^-$ state indicates the disappearance of the $N = 8$ shell closure and the shell evolution in the vicinity of the neutron drip line.

7.3. *Elastic and breakup cross sections of ^{6}He*

Two-neutron halo nuclei such as ^{6}He and ^{11}Li have exotic properties, i.e., soft dipole excitation and a di-neutron correlation. These properties can be investigated via breakup reactions, where the projectile breaks up into three (core+n+n) fragments. For this purpose, accurate description of the four-body systems is essential, and four-body CDCC proposed in §5 is one of the most reliable methods for treating such four-body breakup processes.

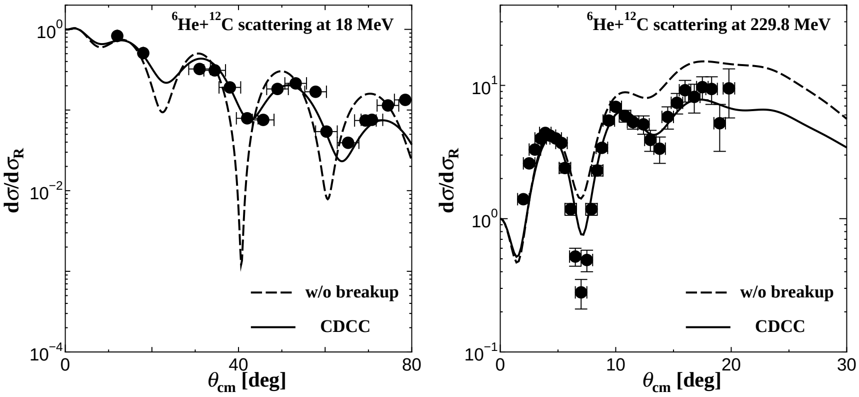

Fig. 17. Angular distributions of the elastic differential cross section for the ^{6}He+^{12}C scattering at 18 MeV (left panel) and 229.8 MeV (right panel). The solid (dashed) line shows the result with (without) breakup effects. The experimental data in the left and right panels are taken from Refs. 130) and 131), respectively.

First, we applied four-body CDCC to the elastic scattering of ^{6}He.$^{48),50)}$ Figure 17 shows the results of the four-body CDCC calculation compared with the experimental data for the ^{6}He+^{12}C scattering at 18 MeV$^{130)}$ and 229.8 MeV.$^{131)}$ In this analysis, coupling potentials in four-body CDCC are calculated by a double-folding model with the density-dependent M3Y interaction$^{132)}$ that has only the real part. The imaginary part of each coupling potential is assumed to have the same form as of the real part with a normalization constant $N_{\rm I}$ to be optimized to reproduce the experimental data. We took $N_{\rm I} = 0.3$ and 0.5 for the scattering at 18 MeV and 229.8 MeV, respectively. One sees clearly from Fig. 17 the importance of the breakup effects; note that $N_{\rm I}$ does not change the oscillation pattern. In this work, we omitted couplings to 1^- continuum states, because the Coulomb breakup effect is negligible in this reaction system.

In Fig. 18, angular distributions of the elastic differential cross section for the ^{6}He+^{209}Bi scattering at 19 MeV and 22.5 MeV$^{133),134)}$ are shown. Since Coulomb breakup effects are dominant in this system, we take into account couplings to 1^- continuum states. In this calculation, we adopt phenomenological optical potentials for the interactions between the ^{209}Bi target and the constituents of ^{6}He. One sees that the four-body CDCC calculation reproduces well the experimental data. Again, the breakup effects are significant. It was found in Ref. 50) also that three-body CDCC, in which a di-neutron plus α structure was assumed for ^{6}He, could not reproduce the data. This shows importance of the accurate description of ^{6}He by means of the three-body model.

Next, four-body CDCC with the new smoothing method described in §5 is applied to analyses of breakup reactions of ^{6}He. In Fig. 19, the calculated breakup

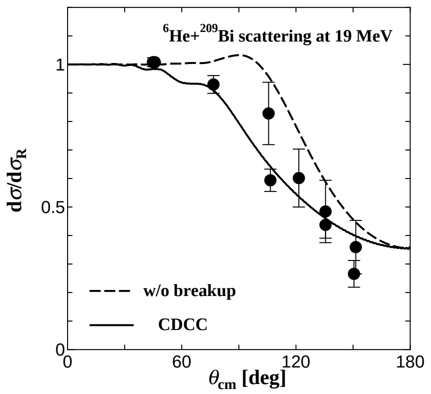

Fig. 18. Same as in Fig. 17 but for the ^{6}He+^{209}Bi scattering at 19 MeV (left panel) and 22.5 MeV (right panel). The experimental data are taken from Refs. 133) and 134).

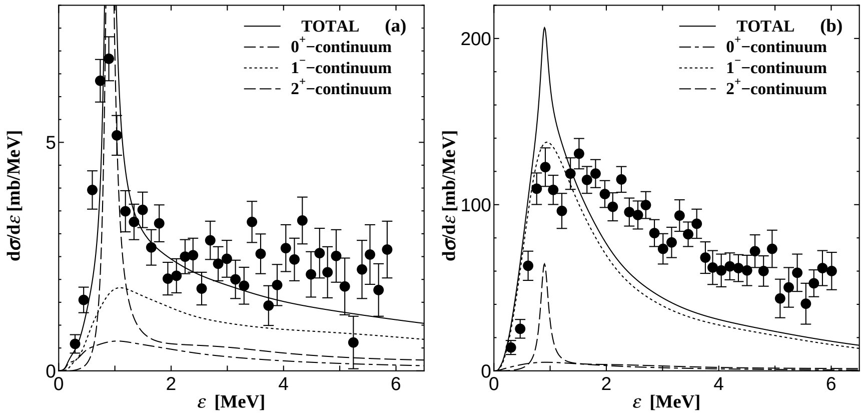

Fig. 19. Comparison of the breakup cross section calculated by CDCC (solid line) with experimental data for (a) the ^{6}He+^{12}C scattering at 240 MeV/nucleon and (b) the ^{6}He+^{208}Pb scattering at 240 MeV/nucleon. The dash-dotted, dotted, and dashed lines correspond to the contributions of the 0^+, 1^-, and 2^+ breakup, respectively, and the solid line is the sum of them. The experimental data are taken from Ref. 124).

cross section $d\sigma/d\varepsilon$ is compared with the experimental data for the ^{6}He+^{12}C and ^{6}He+^{208}Pb reactions at 240 MeV/nucleon.[124)] We found that nuclear breakup was dominant in the former, whereas Coulomb breakup to the 1^- continuum was dominant in the latter. For the ^{12}C target, the present theoretical result is consistent with the experimental data except for the peak of the 2^+ resonance around $\varepsilon = 1$ MeV. For the ^{208}Pb target, the present method undershoots the experimental data for $\varepsilon \gtrsim 2$ MeV. A possible origin of this undershooting is the contribution of the inelastic breakup reactions not included in the present calculation. It was reported in Ref. 135) that the inelastic breakup effect was not negligible, and the elastic breakup cross section calculated with four-body DWBA also underestimated the data.

One of the most important features of these analyses with CDCC is the treatment of the nuclear and Coulomb breakup amplitudes as well as their interference on the same footing. Through a systematic analysis of ^{8}B breakup reactions,$^{41)}$ we showed the importance of the nuclear-Coulomb interference which has been neglected in many studies on breakup of unstable nuclei.

§8. Applications of CDCC to reactions essential in cosmology and astrophysics

In this section, we review our recent applications of CDCC to some reactions important for cosmology and astrophysics. Readers are invited to the references cited in the following subsections for more detailed description of the calculation and complete discussion.

8.1. *Determination of the astrophysical factor S_{17} for the ^{7}Be(p,γ)^{8}B reaction*

Intensive measurements of ^{8}B breakup at intermediate energies$^{136),37),137)}$ have been done to indirectly determine the astrophysical factor $S_{17}(0)$, the value in the zero-energy limit, for the ^{7}Be$(p,\gamma)^{8}$B reaction, which is important for neutrino-physics.$^{138)}$ The results of the indirect measurements of $S_{17}(0)$ are, however, significantly smaller than the result of the precise direct measurement of ^{7}Be$(p,\gamma)^{8}$B.$^{139)}$ This may cast doubt on the reliability of the indirect measurements of astrophysical factors through breakup reactions of unstable nuclei, which are planned to be done at forthcoming RI beam facilities such as FAIR at GSI and FRIB at MSU, and at the brand-new facility RIBF at RIKEN. Thus, to clarify the reason for this discrepancy is a very important subject of nuclearastrophysics. For this purpose we accurately analyzed the ^{8}B breakup by ^{208}Pb at 52 MeV/nucleon with full coupled-channel calculation, i.e., CDCC, taking account of both nuclear and Coulomb breakup with all higher-order processes.$^{46)}$

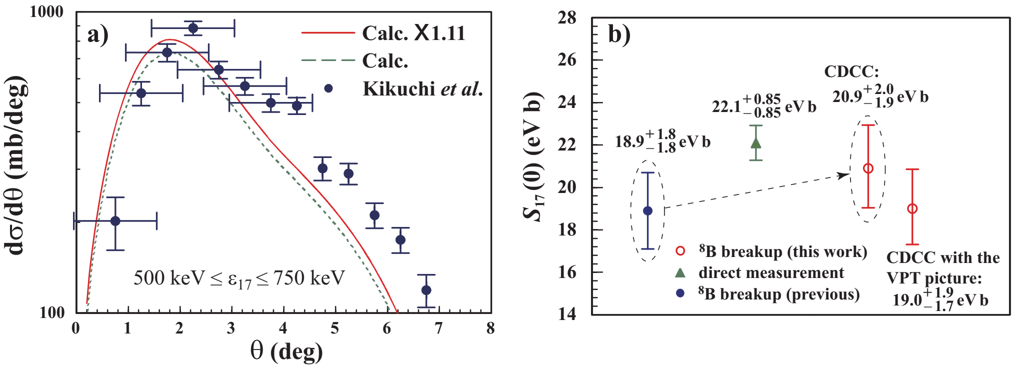

Fig. 20. a) Result of the CDCC analysis of the ^{8}B breakup cross section at 52 MeV/nucleon.$^{136)}$ b) Summary of the present study on $S_{17}(0)$ compared with the previous results. See the text for details.

In the left panel of Fig. 20 we show the result of the CDCC analysis of the ^{8}B breakup cross section by ^{208}Pb at 52 MeV/nucleon.$^{136)}$ The cross section, which is integrated over the relative energy ϵ_{17} of ^{7}Be and p between 500 and 750 keV, is shown as a function of the scattering angle θ of the center-of-mass of ^{8}B (the ^{7}Be+p

system). Numerical inputs for the CDCC calculation are described in Ref. 46) in detail. The dashed line is the result of the calculation using a normalized ^{8}B internal wave function, whereas the solid line is the result of the χ^2 fitting to the experimental data. The theoretical results are smeared out by using a filtering table[140)] to take account of the experimental resolution and efficiency. Since the filtering table was made with assuming the s-state breakup of ^{8}B, which turns out to be valid for $\theta \lesssim 4^\circ$, we use the data in that region in the χ^2-fitting procedure. Note that each horizontal bar put on the data points below 4° does not represent a statistical error but it shows the range of θ in which the breakup cross sections contribute to each data point.[136)] The purpose of the χ^2 fitting is to determine the tail of the overlap function $I(\boldsymbol{r})$ between the ground states of ^{7}Be and ^{8}B, i.e., the asymptotic normalization coefficient (ANC) C; the resulting value of C is 0.74 fm$^{-1/2}$.

It is shown in Ref. 123) that $S_{17}(0)$ for the $^7\mathrm{Be}(p,\gamma)^8\mathrm{B}$ reaction is accurately determined if C is obtained from an alternative reaction in which only the tail region of the overlap function $I(\boldsymbol{r})$ has a significant contribution. We use this so-called ANC method and $S_{17}(0) = 20.9^{+1.0}_{-0.6}$ (theor) ±1.8 (expt) eV b is obtained; the theoretical uncertainties are carefully evaluated by changing the numerical inputs as described in Ref. 46). This value of $S_{17}(0)$ is significantly larger than the previous one, 19.0 ± 1.8 eV b,[136)] which was obtained from the same experimental data as used in the present analysis with the VPT. It is also found that if we assume simple one-step E1 transition in our analysis of the ^{8}B breakup process as in the VPT analysis, $19.0^{+1.9}_{-1.7}$ eV b is obtained,[46)] which agrees very well with the previous result. This clearly shows the importance of the accurate description of the breakup process, taking account of both nuclear and Coulomb breakup with all higher-order processes.

In the right panel of Fig. 20 we summarize the results of the present analysis of the ^{8}B breakup reaction, compared with the results of the precise direct $^7\mathrm{Be}(p,\gamma)^8\mathrm{B}$ measurement[139)] and the previous indirect ^{8}B breakup measurement.[136)] One sees that the agreement between the values of $S_{17}(0)$ obtained from the direct and indirect measurements is significantly improved. It should be noted that very recently, $S_{17}(0) = 20.9 \pm 0.7$ (theor) ±0.6 (expt) eV b was obtained,[141)] as a compilation result of direct measurements, with a small correction to the result of Ref. 139).

Thus, we conclude that the indirect ^{8}B breakup measurement indeed enables accurate determination of the astrophysical factor $S_{17}(0)$ if the breakup reaction is analyzed accurately. This conclusion will be important for a future project to extract nuclearastrophysics information from breakup reactions of unstable nuclei.

8.2. *Three-body model analysis of subbarrier α transfer reaction*

Recently, indirect measurements of $^{13}\mathrm{C}(\alpha,n)^{16}\mathrm{O}$ using subbarrier α transfer reaction $^{13}\mathrm{C}(^6\mathrm{Li},d)^{17}\mathrm{O}(6.356\ \mathrm{MeV},\ 1/2^+)$ has been performed by Florida State University group;[142)] DWBA was used for the analysis of the transfer cross section. ^{6}Li is known to have a $\alpha+d$ two-body structure with a small binding energy of 1.47 MeV. Furthermore, the final state of $^{17}\mathrm{O}(6.356\ \mathrm{MeV},\ 1/2^+)$, which is denoted by $^{17}\mathrm{O}^*$ below for simplicity, locates just 3 keV below the α-^{13}C threshold. Therefore, roles of the breakup states of ^{6}Li and $^{17}\mathrm{O}^*$ in the α transfer process $^{13}\mathrm{C}(^6\mathrm{Li},d)^{17}\mathrm{O}^*$ should be clarified, to obtain a more proper value of the cross section of $^{13}\mathrm{C}(\alpha,n)^{16}\mathrm{O}$ at very low energies.

In this study,[143)] we first calculate with CDCC the elastic cross sections of ^{6}Li-^{13}C at 3.6 MeV and d-$^{17}\mathrm{O}^*$ at 1.1 MeV corresponding to the initial and final channels, respectively, of the $^{13}\mathrm{C}(^6\mathrm{Li},d)^{17}\mathrm{O}^*$ reaction. It is found numerically that the breakup effects of ^{6}Li are important but those of $^{17}\mathrm{O}^*$ are small. Therefore, we evaluate the $^{13}\mathrm{C}(^6\mathrm{Li},d)^{17}\mathrm{O}^*$ cross section at 3.6 MeV including the breakup states of ^{6}Li with CDCC; the transition of the transfer process is described by Born approximation, i.e., we adopt the so-called CDCC-BA framework. In the left panel of Fig. 21, we show the transfer cross section calculated by CDCC-BA with a normalized α-^{13}C wave function (solid line) and that after the χ^2 fitting (dashed line) to the experimental data.[142)] Through this analysis, we obtained 1.03 ± 0.29 fm^{-1} for the square of the Coulomb-modified ANC[142)] of $^{17}\mathrm{O}^*$ with the α-^{13}C configuration, where the second number shows the theoretical and experimental uncertainties together. This result is consistent with the previous result 0.89 ± 0.23 fm^{-1} obtained by the DWBA analysis.[142)] It is found that the transfer processes through the breakup states of ^{6}Li are negligible and only the so-called back-couplings from the breakup states to the ground state of ^{6}Li are important. This means only a proper description of the scattering wave between ^{6}Li and ^{13}C in the elastic channel is necessary. Therefore, use of a reliable optical potential between ^{6}Li and ^{13}C, as in the previous DWBA analysis, may give a proper value of the ANC including the back-coupling effects implicitly. However, this will not always be the case, since usually the optical potential is determined only phenomenologically. Furthermore, breakup transfer processes might be important in other subbarrier α transfer reactions. The present three-body approach, therefore, should be applied systematically to these reactions.

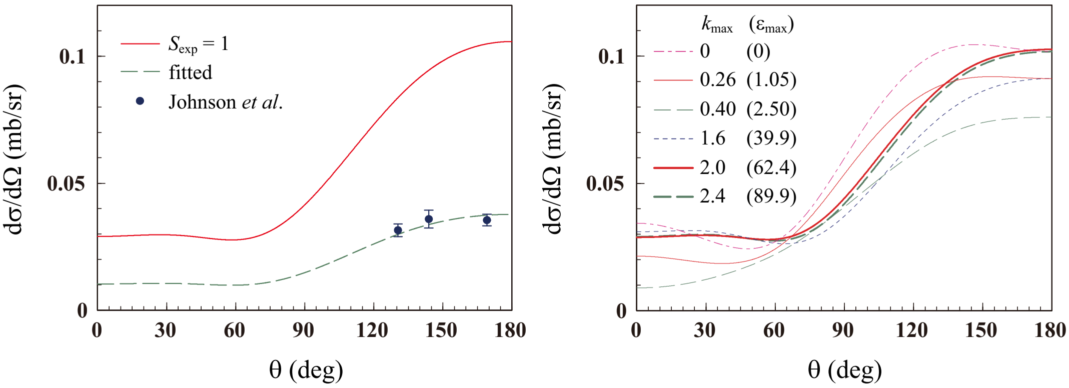

Fig. 21. (left panel) Cross section of the transfer reaction $^{13}\mathrm{C}(^6\mathrm{Li},d)^{17}\mathrm{O}^*$ at 3.6 MeV. The solid line is the result of the calculation with a normalized α-^{13}C wave function and the dashed line is the result of the χ^2 fitting to the experimental data.[142)] (right panel) Dependence of the cross section on the model space of CDCC; see the text for details.

Before ending this subsection, we discuss the convergence of the subbarrier transfer cross section with CDCC. In the right panel of Fig. 21 we show the dependence of the cross section on the maximum value $k_{\max}$ of the relative wave number of the d-α

continuum adopted in CDCC. The values of $k_{\rm max}$ are shown in unit of fm^{-1} and the corresponding values of the d-α relative energy $\epsilon_{\rm max}$ are given in the parentheses in unit of MeV. One sees clearly that the convergence is very slow and obtained eventually at $k_{\rm max} = 2.0$ fm^{-1} ($\epsilon_{\rm max} = 62.4$ MeV). In the usual CDCC calculation, one takes only the open channels, in which the relative energy $E_{\rm rel}$ between the projectile and the target is positive. The result thus obtained (thin solid line) is, however, sizably different from the converged one (thick dotted line). Therefore, inclusion of the closed channels, in which $E_{\rm rel}$ is negative, is necessary for the accurate description of the ^{13}C(^{6}Li, d)^{17}O* reaction at 3.6 MeV with CDCC.

8.3. *Nonresonant triple α process at low temperatures*

Understanding of the formation of ^{12}C, an essential element of life, is one of the most important subjects in physics. It is well known that the so-called triple-α process, i.e., the sequence of the following two reactions

$$\alpha + \alpha \longrightarrow {}^8\mathrm{Be} \Longrightarrow \alpha + {}^8\mathrm{Be} \longrightarrow {}^{12}\mathrm{C}(0_2^+) \longrightarrow {}^{12}\mathrm{C}(2_1^+) + \gamma, \qquad (8\cdot1)$$

is the path to ^{12}C. Particularly, the Hoyle resonance (the second 0^+ state) at 7.65 MeV of ^{12}C plays an essential role in this triple-α process. At low temperatures, say, $T \lesssim 10^8$ K, however, the energy of three α particles cannot reach the Hoyle resonance. In this case, a direct fusion process of three α particles not through the Hoyle resonance becomes dominant. Thus, evaluation of the reaction rate of

$$\alpha + \alpha + \alpha \longrightarrow {}^{12}\mathrm{C}(2_1^+) + \gamma \qquad (8\cdot2)$$

is essential for understanding the formation of ^{12}C.

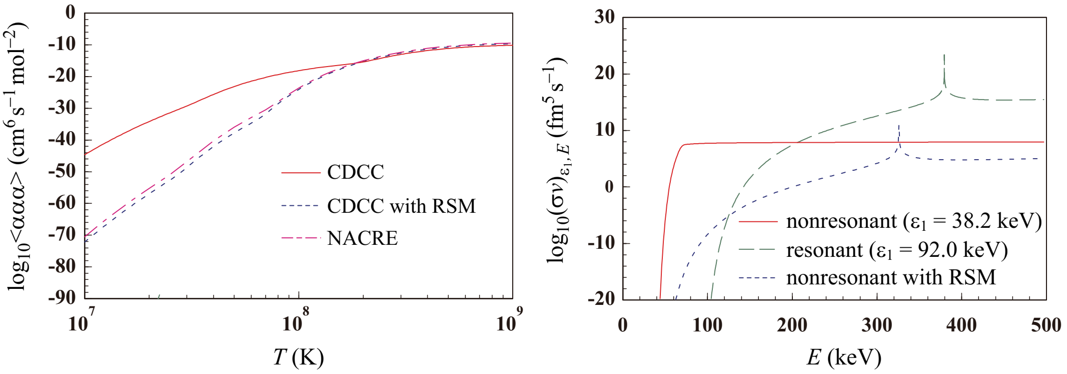

Fig. 22. (left panel) Triple-α reaction rate as a function of temperature. The solid line represents the result of CDCC and the dotted line is the result of CDCC with the RSM. The dash-dotted line shows the reaction rate of NACRE.[145] (right panel) The solid and dashed lines show the reaction probability $(\sigma v)_{\epsilon_1, E}$ of the nonresonant ($\epsilon_1 = 38.2$ keV) and resonant ($\epsilon_1 = 92.0$ keV) processes, respectively. The dotted line shows the result for the nonresonant process with the RSM in the CDCC calculation.

In Ref. 144), formulation of this ternary fusion process (TFP) based on CDCC was developed, and applied to the study of the nonresonant triple-α reaction. We describe resonant and nonresonant processes on the same footing. The left panel of

Fig. 22 shows the resulting reaction rate. The horizontal axis is temperature and the vertical axis is the order of the rate. The solid line is the new reaction rate calculated with CDCC, which is much larger than the rate of NACRE145) shown by the dash-dotted line. The difference is up to about 20 orders of magnitude around 10^7 K. We stress that it is shown in Ref. 144) that the approximate method to mimic the nonresonant triple-α process, the resonance shift method (RSM), proposed by Nomoto146) and used in NACRE, has no theoretical foundation. This can be understood clearly if one sees the reaction probability $(\sigma v)_{\epsilon_1,E}$, where ϵ_1 is the α-α relative energy and E is the total energy of the three-α system. For clear discussion, we show the results of $(\sigma v)_{\epsilon_1,E}$ obtained with the coupled-channel effects switched off; the same model space as in the CDCC calculation converged is adopted. The dashed line in the right panel of Fig. 22 shows $(\sigma v)_{\epsilon_1,E}$ for $\epsilon_1 = 92.0$ keV, i.e., the resonant capture probability. As for nonresonant capture process, we show by the solid line the result for $\epsilon_1 = 38.2$ keV calculated with CDCC, which has completely different energy dependence from that of the dashed line. On the other hand, in the RSM, the probability shown by the dotted line is used. One sees that it has a resonance peak at different energy from that of the Hoyle state ($E = 387$ keV). This is also the case with other values of ϵ_1. Therefore, one finds that the RSM implicitly assumes that there are infinite number of resonances around the Hoyle resonance, which is obviously inconsistent with the experimental information on ^{12}C. If we adopt in our CDCC calculation the assumption used in the RSM (and also in NACRE), we obtain the reaction rate shown by the dotted line in the left panel of Fig. 22 that agrees well with the rate of NACRE.

It should be noted that the calculation of the triple-α reaction at low energies requires extremely large model space as described in Ref. 144). We have confirmed a clear convergence of the reaction rate with respect to the model space of CDCC; the maximum value $r_{\rm max}$ of the α-α relative coordinate r is set to 5,000 fm. If r is truncated at a smaller value, say, 200 fm, we have a reaction rate much smaller than the solid line in the left panel of Fig. 22. This is also the case when a screened Coulomb interaction with a screening radius of a few tens of fm is used.147) It is also found that single-channel calculation never converges, and an adiabatic description of the three-particle system at low energies does not work at all.

Our new reaction rate has been applied to several astrophysics studies.148), 149), 150), 151), 152), 153), 154) Some of them, Refs. 148), 149), 150), 151), show that our reaction rate is incompatible with observation, whereas others, Refs. 152), 153), 154), claim that our rate is consistent with observation; a slight modification on our reaction rate is necessary in Ref. 153). On the nuclear physics side, very recently, a new evaluation of the nonresonant triple-α reaction rate with the hyperspherical harmonic R-matrix method was performed by Nguyen and collaborators.155) They showed that the nonresonant contribution was indeed large, i.e., about 20 orders of magnitude larger than the rate of NACRE at 10^7 K, which is qualitatively consistent with our finding. At temperature higher than 7×10^7 K, however, their result agrees very well with the rate of NACRE. Further investigation on the nonresonant triple-α reaction rate, as well as experimental challenges to reveal the features of the low-energy three-α continuum, will be very important for our understanding of the origin of ^{12}C.

§9. Applications of CDCC to nuclear engineering

One of the advantages of CDCC is its fully quantum-mechanical aspect. Therefore, it is applicable to reactions at low incident energies, which are important for nuclear engineering. In this section, we show some results of applications of CDCC to studies in this field.

9.1. *Deuteron induced reactions on* $^{6,7}Li$

In the international fusion material irradiation facility (IFMIF) project,156) deuteron induced reactions on ^{6,7}Li are considered as one of the most promising reactions to generate high-intensity neutrons. Understanding of the ^{6,7}Li(d,xn) processes, where x indicates all possible reaction products, at incident energies up to 50 MeV is highly important. Neutron spectra observed at forward angles show a broad peak with approximately half the incident energy.157) This suggests an importance of deuteron breakup processes, namely, deuteron dissociation and proton stripping due to nuclear fields. In the past works,158),159) these processes were treated using semi-classical models such as the modified intra-nuclear cascade (INC) model158) and the Serber model.160) Since the incident energy of interest here is relatively low, more sophisticated quantum mechanical approaches will be necessary for quantitative understanding of the neutron production rate.

The ^{6,7}Li(d,xn) cross sections are expected to consist of the contributions from the deuteron elastic breakup and proton stripping processes. In Ref. 161) we applied CDCC and the Glauber model15) to estimate the former and the latter, respectively, of the ^{7}Li(d,xn) reaction at 40 MeV. As for the nucleon optical model potential for ^{7}Li, we took the parameter set determined in Ref. 162) through a systematic analysis of the nucleon elastic scattering on ^{6,7}Li.

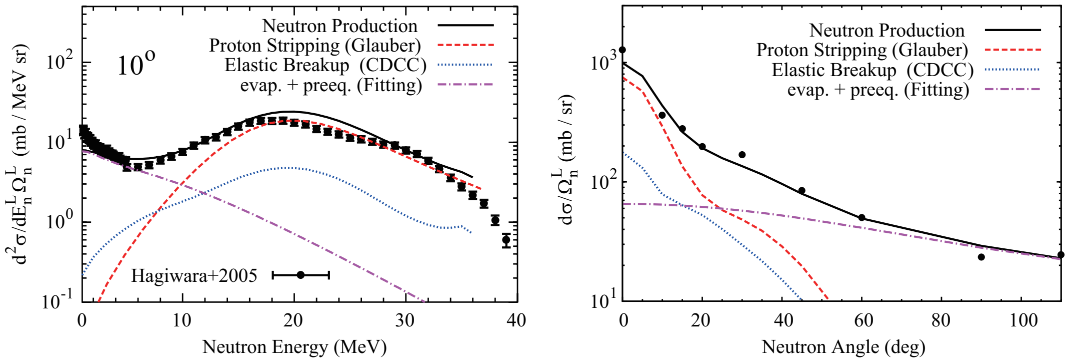

Fig. 23. Comparison between the experimental data and the calculated result of $d^2\sigma/(dE_n^{\rm L} d\Omega_n^{\rm L})$ at the neutron emission angle 10° (left panel) and the neutron angular distribution (right panel) of ^{7}Li(d,xn) at 40 MeV. For the latter, the cross section is integrated over the neutron outgoing energies. The proton stripping and elastic breakup components are plotted by the dashed and dotted lines, respectively, and the sum of the evaporation and pre-equilibrium components is shown by the dash-dotted line. The solid line represents the total neutron production.

In Fig. 23 we show the comparison between the calculated result and the experimental data. The left panel shows the double differential breakup cross section

$d^2\sigma/(dE_n^{\rm L} d\Omega_n^{\rm L})$ with respect to the energy $E_n^{\rm L}$ and the angle $\Omega_n^{\rm L}$ of the outgoing neutron in the laboratory frame; the result corresponds to the neutron scattering angle at 10°. The angular distribution $d\sigma/d\Omega_n^{\rm L}$ is shown in the right panel. In each panel, the solid and dashed lines show, respectively, the contributions of the elastic breakup and the stripping. The dotted line is the sum of the evaporation and pre-equilibrium components, which are evaluated by an empirical method, i.e., the moving source model.$^{161)}$

The calculation reproduces the experimental data quite well. As expected, the deuteron breakup processes are strongly involved with the formation of the bump around 20 MeV of the outgoing neutron energy. The proton stripping process is more predominant than the elastic breakup process. It is worth noting that the strong contribution from the stripping process is also indicated by the DWBA calculation for (d, px) reactions on medium-heavy nuclei at 25.5 MeV.$^{163)}$ The relative contribution from the stripping process is reduced as the angle increases. It is found also that the deuteron breakup processes dominate neutron production at forward angles and are negligible at backward angles, while the evaporation and pre-equilibrium processes have a major contribution at backward angles. Consequently, the present analysis suggests that accurate description of the deuteron breakup reactions including both the elastic breakup and proton stripping processes is essential for reliable design of the neutron sources using the ^{7}Li(d, xn) reaction.

Although this model calculation reproduces successfully well the experimental data at small angles, we found some problems of the Glauber model calculation for the neutron stripping. The Glauber model calculation shows that the peak position in the emission spectra shifts to high energy as the emission angle increases, and fails to reproduce the experimental spectra at large angles; see Ref. 161). Furthermore, inclusive (d, xp) spectra for heavy target nuclei are underestimated by the model calculation$^{164)}$ because the Glauber model cannot treat Coulomb breakup effects accurately. These may suggest a limitation of applying the Glauber model. Therefore, it is desirable to apply the eikonal reaction theory (ERT) described in §6 to the evaluation of the stripping process. This may eventually make it feasible to *predict* nucleon production from deuteron induced reactions.

9.2. *Neutron induced reactions on ^{6}Li*

Lithium isotopes will be used as a tritium-breeding material in *d*-*t* fusion reactors, and accurate nuclear data are required for *n*- and *p*-induced reactions. Indeed, the international atomic energy agency (IAEA) is organizing a research coordination meeting to prepare nuclear data libraries for advanced fusion devices, FENDL-3,$^{165)}$ and the maximum incident energy is set to 150 MeV to comply fully with the requirements for the IFMIF project. Lithium isotopes are some of the most important materials in these libraries. In fact, understanding of the breakup properties of lithium isotopes by neutron is crucial to determine the neutron energy spectra in blankets of fusion reactors. The tritium breeding ratio, nuclear heating distributions, and radiation damage of structural materials are affected by the n+Li reactions significantly.

In spite of the importance of the n+^{6}Li reaction mentioned above, experimental data of the breakup processes leading to the ^{6}Li continuum are extremely rare for the neutron energy region above 20 MeV. Furthermore, the statistical model, often used in evaluation of nuclear data for medium to heavy nuclei, cannot be applied to the $^6\mathrm{Li}(n,n')$ reactions. As mentioned in Refs. 166) and 167), the mechanisms leading to the three-body $(n+d+\alpha)$ and four-body $(n+n+p+\alpha)$ final states are particularly important. Therefore, more reliable theoretical calculations for the cross sections are highly desirable.

In Ref. 168), we performed a microscopic analysis of n+^{6}Li scattering by means of CDCC. In this analysis, ^{6}Li is described as a $d+\alpha$ system, and the interaction between n and ^{6}Li is calculated by a folding model with the JLM effective interaction,$^{74)}$ where the normalization of the imaginary part, λ_w, is optimized to reproduce the elastic cross sections. Details of the calculation are shown in Ref. 168).

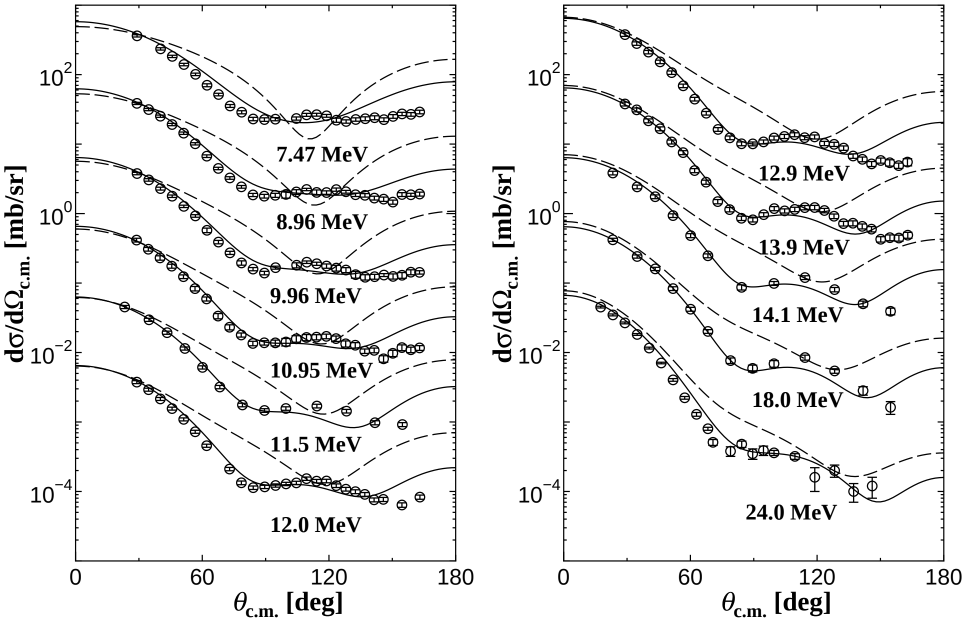

Fig. 24. Angular distribution of the elastic differential cross section of n+^{6}Li scattering for incident energies between 7.47 and 24.0 MeV. The solid and dashed lines correspond to the result with and without couplings to breakup states of ^{6}Li, respectively. Experimental data are taken from Refs. 169), 170), 171). The results are subsequently shifted downward by a factor of 10^{-1}–10^{-5} from 8.96 MeV to 12.0 MeV on the left panel, and 10^{-1}–10^{-4} from 13.9 MeV to 24.0 MeV on the right panel, respectively.

Figure 24 shows the differential elastic cross sections of n+^{6}Li for incident energies between 7.47 and 24.0 MeV. One sees that the results of the CDCC calculation (the solid lines) are in good agreement with the experimental data. The dashed lines represent the results of a single-channel calculation, in which couplings to the breakup states are omitted. It is found that breakup effects shown by the difference between the dashed and solid lines are significant to reproduce the angular distributions of the elastic scattering. For all incident energies, we take $\lambda_w = 0.1$ to reproduce the data. It should be noted that the single-channel calculation cannot reproduce the experimental data with any values of λ_w. The very small value of λ_w obtained may indicate that most of the reaction channels that cause loss of the incident flux are treated explicitly in the CDCC calculation.

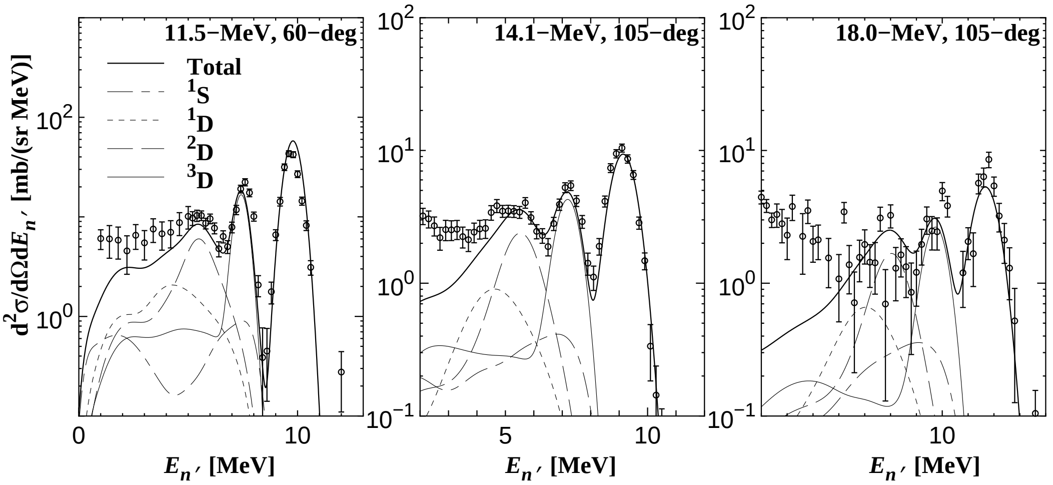

Fig. 25. The neutron spectra calculated by CDCC with the JLM interaction comparing with measured data at selected angular points in the laboratory system. The experimental data are taken from Ref. 169).

In Fig. 25, the calculated neutron spectra are compared with the experimental data at selected scattering angles in the laboratory frame and incident energies; λ_w is fixed at 0.1. Components of the breakup states of ^{1}S, ^{1}D, ^{2}D, and ^{3}D are represented by the dash-dotted, dashed, dotted, and thin solid lines, respectively. These results are broadened by considering the finite resolution of the experimental apparatus.[169)] In each panel, three peaks of the experimental data correspond to the elastic scattering (right), the inelastic scattering to the 3^+ resonance (center), and the inelastic scattering to the 2^+ resonance (left). The CDCC calculation gives a good agreement with experimental data in the high neutron energy region. On the other hand, in the low neutron energy region, which corresponds to highly exited states of ^{6}Li, the calculated cross section considerably undershoot the experimental data. This indicates that experimental data contain contribution from the $(n, 2n)$ process due to a four-body breakup reaction ^{6}Li$(n, nnp)\alpha$, as indicated in Ref. 169). In the present calculation, the four-body breakup effects are treated only implicitly by using a complex optical potential. Estimate of these effects with four-body CDCC will be very important.

Thus, CDCC with the JLM interaction is expected to be a powerful framework for the data evaluation of the ^{6}Li(n, n') reactions. Once the JLM parameter is determined by an analysis of elastic scattering, evaluation of the inelastic cross sections and neutron breakup spectra can be done with no free adjustable parameters. This is a very important feature of the present framework that enables a quantitative calculation of the cross sections for nuclear engineering studies.

§10. Summary

This review has shown recent developments of the continuum discretized coupled-channels method (CDCC) and its applications to nuclear physics, cosmology and astrophysics, and nuclear engineering, after the previous review articles of Refs. 24) and 25).

First, we have shown the theoretical foundation of CDCC. The primary approximation in CDCC is the truncation of the angular momentum ℓ between two constituents of the projectile. This ℓ-truncation changes the two-body potentials between the target and the constituents to three-body potentials. The CDCC solution is the zeroth-order solution to the distorted Faddeev equations with the three-body potentials, the first-order correction to which is largely suppressed. The CDCC solution is thus a good solution to the three-body Schrödinger equation, when the maximum value of ℓ is large enough. This theoretical statement has recently been confirmed numerically by directly comparing the CDCC and Faddeev solutions.66) In CDCC calculations, it is necessary to confirm the convergence of the solution with respect to expanding the model space, so that the CDCC solution has no model space dependence and hence is a good solution to the three-body Schrödinger equation.

As an underlying theory of CDCC, we have constructed a microscopic reaction theory for nucleus-nucleus scattering based on the multiple scattering theory. The input of the theory is either the t- or the g-matrix NN interaction instead of the realistic one. The former has much milder r dependence, so that the Glauber model becomes reliable for the systems in which the Coulomb interactions are weak, when either the t- or the g-matrix is used as an input of the model. In the scattering of lighter projectiles from lighter targets at intermediate energies, effects induced by finite nucleus such as projectile breakup and target collective excitations are found to be small. Then the double-folding model becomes reliable for the scattering. Using the model, one can construct the microscopic optical potential with projectile and target densities calculated by fully microscopic structure theories such as antisymmetrized molecular dynamics (AMD), the Hartree-Fock (HF) method, and the Hartree-Fock-Bogoliubov (HFB) method. This fully microscopic framework has been applied to the scattering of stable nuclei and unstable neutron-rich Ne isotopes at intermediate energies with success in reproducing experimental data. The reliable microscopic optical potential can be used as an input of CDCC calculations, since the nonlocal potential can be localized with the Brieva-Rook (BR) method accurately. This microscopic version of CDCC is quite useful to analyze scattering of unstable nuclei systematically.

Then we have extended CDCC in three directions, and developed the following new frameworks for breakup reactions: i) *eikonal-CDCC (E-CDCC)* for Coulomb-dominated breakup processes, ii) *four-body CDCC* for breakup of a three-body projectile, and iii) *the eikonal reaction theory (ERT)* for inclusive breakup processes.

E-CDCC treats both nuclear and Coulomb breakup very accurately and efficiently. The quantum-mechanical (QM) corrections, if necessary, can be made by replacing the partial scattering amplitudes corresponding to small impact parameters b with the solutions of a QM calculation, i.e., CDCC. E-CDCC calculations with the QM corrections are much faster than CDCC calculations, with keeping the same accuracy as the latter. E-CDCC has thus become a standard method for describing breakup reactions in which the Coulomb breakup contribution is essential. Recently, inclusion of a relativistic Liénard-Wiechert potential as a Coulomb interaction was accomplished in E-CDCC, and dynamical relativistic effects generated by the potential were found to give a sizable increase in the ^{8}B and ^{11}Be breakup cross sections at 250 MeV/nucleon.

Four-body CDCC adopts pseudostates, which are obtained by diagonalizing the internal Hamiltonian of a three-body projectile, as discretized-continuum states of the projectile. The four-body wave function is expanded by the pseudostates together with the bound state(s); they are assumed to form a complete set in a space in which the reaction takes place. Additionally, a new method for obtaining a smooth breakup energy spectrum from discrete breakup cross sections given by CDCC was proposed. Four-body CDCC together with this new smoothing method based on the complex-scaling method has completed the description four-body breakup processes. Clear convergence with respect to expanding the model space is seen in both the elastic and the breakup cross section of the ^{6}He scattering, and the results converged are consistent with experimental data. Four-body CDCC with the new smoothing method is indispensable for systematic studies of unstable nuclei that have a three-body structure.

ERT is a framework that makes CDCC applicable to inclusive breakup processes such as neutron removal reactions, in which only the core nucleus of the projectile is detected. ERT gives separation of the scattering matrix into the contribution of each constituent of the projectile, without making the adiabatic approximation to the Coulomb potential. This is an essential point of ERT that eliminates the well-known shortcoming of the Glauber model, i.e., the divergence problem in Coulomb breakup. ERT has been successfully applied to the one-neutron removal from ^{31}Ne, and one- and two-neutron removal from ^{6}He. With ERT, the accuracy of the Glauber model was systematically investigated for deuteron induced reactions at 200 MeV/nucleon. The Glauber model is good for light targets, but not for heavier targets, because of the Coulomb breakup contributions for the latter.

CDCC, E-CDCC, four-body CDCC, ERT, and the microscopic version of CDCC have extensively and successfully been applied to studies of various reactions essential in nuclear physics, cosmology and astrophysics, and nuclear engineering. These methods treat nuclear and Coulomb breakup processes nonperturbatively and nonadiabatically, and have no free adjustable parameters. These features are essential for *quantitative* studies such as the investigation of four-body breakup properties of ^{6}He at the Coulomb barrier energy, determination of astrophysical S factors, evaluation of the contribution from the nonresonant triple-α process, the accurate estimation of neutron yields for the nuclear engineering design, and so forth. Validation of findings or conjectures obtained by nuclear structural studies through direct comparison with experimental cross sections is also highly important. The microscopic reaction theory plays definitely important roles in this subject, as we have confirmed ^{31}Ne to be a halo nucleus with large deformation.

There are several interesting future works based on CDCC and the extended theories. One is systematic applications of these theories to nuclear physics and the related fields. Another interesting work is to clarify the relation between CDCC and the dynamical eikonal approximation (DEA).60),61) Many nuclei can be described well by a core nucleus and extra nucleon(s). In the scattering of these nuclei, excitations of the core nucleus are important in general.172),173) It is interesting to extend CDCC to treat the core excitations during the breakup. Use of other three-body structural models in four-body CDCC is also an important future work. The cluster-orbital shell model (COSM),174),175) which has been applied to up to five-body systems, is one of the most promising models. Extension of four-body CDCC to five- and six-body CDCC with COSM will be a very attractive subject to explorer drip line nuclei. Finally, it will be very important to develop more accurate description of transfer reactions at relatively low energies, by treating the rearrangement channels nonperturbatively. This will be essential to investigate excited states of stable and unstable nuclei, which are to be accessed via transfer reactions. These future works are important in further development of nuclear physics and the related fields.

Acknowledgement

This review is based on the collaboration with C. A. Bertulani, S. Chiba, T. Egami, T. Fukui, S. Hashimoto, Y. Hirabayashi, E. Hiyama, D. Ichinkhorloo, Y. Iseri, M. Kamimura, T. Kamizato, M. Kan, K. Katō, M. Kawai, M. Kimura, M. Kohno, Y. Kondo, T. Nakamura, R. A. D. Piyadasa, Y. R. Shimizu, T. Sumi, S. Tagami, S. Watanabe, Y. Watanabe, and T. Ye. The authors wish to sincerely thank these people. The authors also deeply appreciate D. Baye, P. Capel, P. Descouvemont, M. Fukuda, T. Furumoto, K. Hagino, T. Kajino, A. M. Moro, T. Motobayashi, G. V. Rogachev, Y. Sakuragi, H. Sakurai, Y. Suzuki, M. Takechi, and K. Yabana for valuable suggestions and fruitful discussions. This work has been supported in part by the Grants-in-Aid for Scientific Research from Japan Society for the Promotion of Science. The computation was carried out using mainly the computer facilities at the Research Institute for Information Technology, Kyushu University.

References

1) I. Tanihata, *et al.*, Phys. Lett. B **289** (1992), 261.
I. Tanihata, J. Phys. G **22** (1996), 157.
2) A. S. Jensen, *et al.*, Rev. Mod. Phys. **76** (2004), 215.
3) B. Jonson, Phys. Rep. **389** (2004), 1.
4) E. K. Warburton, J. A. Becker, and B. A. Brown, Phys. Rev. C **41** (1990), 1147.
5) T. Motobayashi *et al.*, Phys. Lett. B **346** (1995), 9.
6) E. Caurier, F. Nowacki, A. Poves, J. Retamosa, Phys. Rev. C **58** (1998), 2033.
7) Y. Utsuno, T. Otsuka, T. Mizusaki, M. Honma, Phys. Rev. C **60** (1999), 054315.
8) H. Iwasaki *et al.*, Phys. Lett. B **522** (2001), 227.
9) Y. Yanagisawa *et al.*, Phys. Lett. B **566** (2003), 84.
10) A. Gade, *et al.*, Phys. Rev. C **77** (2008), 044306.
11) M. Takechi *et al.*, Nucl. Phys. **A834** (2010), 412c.
12) T. Nakamura, *et al.*, Phys. Rev. Lett. **103** (2009), 262501.
13) K. M. Watson, Phys. Rev. **89** (1953), 575.
14) A. K. Kerman, H. McManus, and R. M. Thaler, Ann. Phys. **8** (1959), 551.

15) R.J. Glauber, *in Lectures in TheoreticalPhysics* (Interscience, New York, 1959), Vol. 1, p.315.
16) M. S. Hussein and K. W. McVoy, Nucl. Phys. A **445** (1985), 124.
17) K. Hencken, G. Bertsch, and H. Esbensen, Phys. Rev. C **54** (1996), 3043.
18) K. Yabana, Y. Ogawa, and Y. Suzuki, Nucl. Phys. A **539** (1992), 295; Y. Ogawa, K. Yabana, and Y. Suzuki, Nucl. Phys. A **543** (1992), 722; Y. Ogawa, T. Kido, K. Yabana, and Y. Suzuki, Prog. Theor. Phys. Supplement **142** (2001), 157.
19) J.S. Al-Khalili and J.A. Tostevin, Phys. Rev. Lett. **76** (1996), 3903; J.A. Tostevin and B.A. Brown, Phys. Rev. C **74** (2006), 064604.
20) C. A. Bertulani and K. W. McVoy, Phys. Rev. C **46** (1992), 2638.
21) C. A. Bertulani and P. G. Hansen, Phys. Rev. C **70** (2004), 034609.
22) B. Abu-Ibrahim and Y. Suzuki, Prog. Theor. Phys. **112** (2004), 1013; B. Abu-Ibrahim and Y. Suzuki, Prog. Theor. Phys. **114** (2005), 901.
23) P. Capel, D. Baye, and Y. Suzuki, Phys. Rev. C **78** (2008), 054602.
24) M. Kamimura, M. Yahiro, Y. Iseri, Y. Sakuragi, H. Kameyama, and M. Kawai, Prog. Theor. Phys. Suppl. **89** (1986), 1.
25) N. Austern, Y. Iseri, M. Kamimura, M. Kawai, G. Rawitscher, and M. Yahiro, Phys. Rep. **154** (1987), 125.
26) Y. Hirabayashi, Phys. Rev. C **44** (1991), 1581.
27) K. Rusek and K.W. Kemper, Phys. Rev. C **61** (2000), 034608.
28) Y. Hirabayashi and Y. Sakuragi, Phys. Rev. Lett. **69** (1991), 1892; Erratum: Y. Hirabayashi and Y. Sakuragi, Phys. Rev. Lett. 69, 3000 (1992).
29) A. Diaz-Torres, I. J. Thompson, and C. Beck. Phys. Rev. C **68** (2003), 044607.
30) P. R. S. Gomes *et al.*, Phys. Rev. C **71** (2005), 034608.
31) C. Beck, N. Keeley, and A. Diaz-Torres, Phys. Rev. C **75** (2007), 054605.
32) K. Rusek, N. Alamanos, N. Keeley, V. Lapoux, and A. Pakou, Phys. Rev. C **70** (2004), 014603.
33) K. Rusek, I. Martel, J. Gómez-Camacho, A.M. Moro, and R. Raabe, Phys. Rev. C **72** (2005), 037603.
34) A. M. Moro, K. Rusek, J. M. Arias, J. Gomez-Camacho, and M. Rodriguez-Gallardo, Phys. Rev. C **75** (2007), 064607.
35) P. N. de Faria *et al.*, Phys. Rev. C **81** (2010), 044605.
36) J. A. Tostevin, F. M. Nunes, and I. J. Thompson, Phys. Rev. C **63** (2001), 024617.
37) B. Davids *et al.*, Phys. Rev. C **63** (2001), 065806.
38) A. M. Moro, R. Crespo, F. Nunes, and I. J. Thompson, Phys. Rev. C **66** (2002), 024612.
39) A. M. Moro and F. M. Nunes, Nucl. Phys. A **767** (2006), 138.
40) M. S. Hussein, R. Lichtenthaler, F. Nunes, and I. J. Thompson, Phys. Lett. B **640** (2006), 91.
41) K. Ogata, T. Matsumoto, Y. Iseri, and M. Yahiro, J. Phys. Soc. Jpn. **78** (2009), 084201.
42) A. Diaz-Torres and I. J. Thompson, Phys. Rev. C **65** (2002), 024606.
43) M. Takashina, S. Takagi, Y. Sakuragi, and Y. Iseri, Phys. Rev. C **67** (2003), 037601.
44) L. F. Canto, J. Lubian, P. R. S. Gomes, and M. S. Hussein, Phys. Rev. C **80** (2009), 047601.
45) K. Ogata, M. Yahiro, Y. Iseri, T. Matsumoto and M. Kamimura, Phys. Rev. C **68** (2003), 064609.
46) K. Ogata, S. Hashimoto, Y. Iseri, M. Kamimura and M. Yahiro, Phys. Rev. C **73** (2006), 024605.
47) T. Matsumoto, T. Kamizato, K. Ogata, Y. Iseri, E. Hiyama, M. Kamimura, and M. Yahiro, Phys. Rev. C **68** (2003), 064607.
48) T. Matsumoto, E. Hiyama, K. Ogata, Y. Iseri, M. Kamimura, S. Chiba, and M. Yahiro, Phys. Rev. C **70** (2004), 061601(R).
49) T. Egami, K. Ogata, T. Matsumoto, Y. Iseri, M. Kamimura, and M. Yahiro, Phys. Rev. C **70** (2004), 047604.
50) T. Matsumoto, T. Egami, K. Ogata, Y. Iseri, M. Kamimura, and M. Yahiro, Phys. Rev. C **73** (2006), 051602(R).
51) T. Egami, T. Matsumoto, K. Ogata, and M. Yahiro, Prog. Theor. Phys. **121** (2009), 789.
52) T. Matsumoto, T. Egami, K. Ogata, and M. Yahiro, Prog. Theor. Phys. **121** (2009), 885.
53) T. Matsumoto, K. Katō, and M. Yahiro, Phys. Rev. C **82** (2010), 051602.

54) A. M. Moro, J. M. Arias, J. Gómez-Camacho, I. Martel, F. Pérez-Bernal, R. Crespo and F. Nunes, Phys. Rev. C **65** (2001), 011602(R).
55) M. Rodríguez-Gallardo *et al.*, Phys. Rev. C **72** (2005), 024007.
56) A. M. Moro, F. Perez-Bernal, J. M. Arias, and J. Gomez-Camacho, Phys. Rev. C **73** (2006), 044612.
57) M. Rodríguez-Gallardo, J. M. Arias, J. Gómez-Camacho, R. C. Johnson, A. M. Moro, I. J. Thompson, and J. A. Tostevin, Phys. Rev. C **77** (2008), 064609.
58) A. M. Moro, J. M. Arias, J. Gomez-Camacho, and F. Perez-Bernal, Phys. Rev. C **80** (2009), 054605.
59) M. Rodríguez-Gallardo, J. M. Arias, J. Gómez-Camacho, A. M. Moro, I. J. Thompson, and J. A. Tostevin, Phys. Rev. C **80** (2009), 051601(R).
60) D. Baye, P. Capel, and G. Goldstein, Phys. Rev. Lett. **95** (2005), 082502;
61) G. Goldstein, D. Baye, and P. Capel, Phys. Rev. C **73** (2006), 024602.
62) M. Yahiro, K. Minomo, K. Ogata, and M. Kawai, Prog. Theor. Phys. **120** (2008), 767.
63) F.A. Brieva and J.R. Rook, Nucl. Phys. A**291**, 299 (1977); ibid. 291, 317 (1977); ibid. 297, 206 (1978).
64) N. Austern, M. Yahiro, and M. Kawai, Phys. Rev. Lett. **63** (1989), 2649.
65) N. Austern, M. Kawai, and M. Yahiro, Phys. Rev. C **53** (1996), 314.
66) A. Deltuva, A. M. Moro, E. Cravo, F. M. Nunes, and A. C. Fonseca, Phys. Rev. C **76** (2007), 064602.
67) R. A. D. Piyadasa, M. Yahiro, M. Kamimura and M. Kawai, Prog. Theor. Phys. **81** (1989), 910.
68) R. A. D. Piyadasa, M. Kawai, M. Kamimura and M. Yahiro, Phys. Rev. C **60** (1999), 044611.
69) R. Y. Rasoanavio and G. H. Rawitscher, Phy. Rev. C **39** (1989), 1709.
70) M.C. Birse and E. F. Redish, Nucl. Phys. A**406** (1982), 149.
71) G. Takeda and K. M. Watson, Phys. Rev. **97** (1955), 1336.
72) A. Picklesimer and R. M. Thaler, Phys. Rev. C**23** (1981), 42.
73) G. Bertsch, J. Borysowicz, M. McManus, and W. G. Love, Nucl. Phys. A**284** (1977), 399.
74) J.-P. Jeukenne, A. Lejeune, and C. Mahaux, Phys. Rev. C**16**, 80 (1977); ibid. Phys. Rep. **25** (1976), 83.
75) G. R. Satchler, Phys. Rep. **55** (1979), 183-254.
76) G. R. Satchler, "Direct Nuclear Reactions", Oxfrod University Press, (1983).
77) N. Yamaguchi, S. Nagata and T. Matsuda, Prog. Theor. Phys. **70** (1983), 459; N. Yamaguchi, S. Nagata and J. Michiyama, Prog. Theor. Phys. **76** (1986), 1289.
78) L. Rikus, K. Nakano and H. V. von Geramb, Nucl. Phys. A**414** (1984), 413; L. Rikus and H.V. von Geramb, Nucl. Phys. A**426** (1984), 496.
79) K. Amos, P. J. Dortmans, H. V. von Geramb, S. Karataglidis, and J. Raynal, in *Advances in Nuclear Physics*, edited by J. W. Negele and E. Vogt(Plenum, New York, 2000) Vol. 25, p. 275.
80) T. Furumoto, Y. Sakuragi, and Y. Yamamoto, Phys. Rev. C**78**, 044610 (2008); *ibid.*, C**79** (2009), 011601(R); *ibid.*, C**80** (2009), 044614.
81) R. B. Wiringa, V. G. J. Stoks and R. Schiavilla, Phys. Rev. C**51** (1995), 38.
82) R.J. Glauber and G. Matthiae, Nucl. Phys. B**21** (1970), 135.
83) D. J. Ernst, J. T. Londergan, G. A. Miller, and R. M. Thaler, Phys. Rev. C **16** (1977), 537; E. R. Siciliano and R. M. Thaler, Phys. Rev. C **16** (1977), 1322; P. C. Tandy and R. M. Thaler Phys. Rev. C **22** (1980), 2321.
84) C. R. Chinn, Ch. Elster, R. M. Thaler, and S. P. Weppner, Phys. Rev. C **51** (1995), 1418; C. R. Chinn, Ch. Elster, R. M. Thaler, and S. P. Weppner, Phys. Rev. C **52** (1995), 1992; Ch. Elster, S. P. Weppner, and C. R. Chinn Phys. Rev. C **56** (1997), 2080; S. P. Weppner, Ch. Elster, and D. Huber, Phys. Rev. C **57** (1998), 1378.
85) P. K. Deb and K. Amos, Phys. Rev. C **62** (2000), 024605.
86) H. Sakaguchi *et al.*, Phys. Rev. C **26** (1982), 944.
87) F. T. Baker *et al.*, Nucl. Phys. A **393** (1983), 283.
88) K. Minomo, K. Ogata, M. Kohno, Y. R. Shimizu and M. Yahiro, J. Phys. G **37** (2010), 085011 [arXiv:0911.1184 [nucl-th]].
89) F. Perrey and B. Buck, Nucl. Phys. **32** (1962), 353.
90) B. Sinha, Phys. Rep. **20** (1975), 1.

B. Sinha and S. A. Moszkowski, Phys. Lett. B**81** (1979), 289.

91) T. Furumoto, Y. Sakuragi, and Y. Yamamoto, Phys. Rev. C**82** (2010), 044612.

92) H. de Vries, C. W. de Jager, and C. de Vries, At. Data Nucl. Data Tables **36** (1987), 495.

93) T. Ichihara *et al.*, Nucl. Phys. A**569** (1994), 287c-296c.

94) W. G. Love and M. A. Franey, Phys. Rev. C**24** (1981), 1073; M. A. Franey and W. G. Love, Phys. Rev. C**31** (1985), 488.

95) T. Suzuki *et al.*, Phys. Rev. Lett. **75** (1995), 3241.

96) L. Chulkov *et al.*, Nucl. Phys. A**603** (1996), 219.

97) M. Takechi, *et al.*, Phys. Rev. C **79** (2009), 061601(R).

98) M. Kimura and H. Horiuchi, Prog. Theor. Phys. **111** (2004), 841; M. Kimura, Phys. Rev. C **75** (2007), 041302. M. Kimura, arXiv:1105.3281 (2011) [nucl-th].

99) J. Decharge and D. Gogny, Phys. Rev. C **21** (1980), 1568.

100) J. F. Berger, M. Girod, and D. Gogny, Comp. Phys. Comm. **63** (1991), 1365.

101) K. Minomo, T. Sumi, M. Kimura, K. Ogata, Y. R. Shimizu and M. Yahiro, Phys. Rev. Lett. **108** (2012), 052503.

102) K. Minomo, T. Sumi, M. Kimura, K. Ogata, Y. R. Shimizu, and M. Yahiro, Phys. Rev. C **84** (2011), 034602.

103) T. Sumi *et al.*, arXiv:1201.2497 [nucl-th].

104) for a review, C. A. Bertulani, arXiv0908.4307 (2009).

105) J. D. Jackson, "Classical Electrodynamics" (New York: Wiley), 1975.

106) C. A. Bertulani and G. Baur, Phys. Rep. **163** (1988), 299.

107) K. Ogata and C. A. Bertulani, Prog. Theor. Phys. **121** (2009), 1399.

108) K. Ogata and C. A. Bertulani, Prog. Theor. Phys. **123** (2009), 701.

109) C. A. Bertulani, Phys. Rev. Lett. **94** (2005), 072701.

110) H. Feshbach and M. Zabek, Ann. of Phys. **107** (1977) 110.

111) I. Thompson, F. Nunes, and B. Danilin, Comput. Phys. Commun. **161** (2004), 87.

112) J. Aguilar and J. M. Combes, Commun. Math. Phys. **22** (1971), 269; E. Balslev and J. M. Combes, Commun. Math. Phys. **22** (1971), 280.

113) T. Myo, A. Ohnishi, and K. Katō, Prog. Theor. Phys. **99**, 801 (1998).

114) Y. Suzuki, W. Horiuchi, and D. Baye, Prog. Theor. Phys. **123**, 547 (2010).

115) D. Gogny, P. Pires, and R. de Tourreil, Phys. Lett. B **32** (1970), 591.

116) H. Kanada, T. Kaneko, S. Nagata, and M. Nomoto, Prog. Theor. Phys. **61** (1979), 1327.

117) S. Saito, Prog. THeor. Phys. **41** (1969), 705.

118) E. Hiyama, Y. Kino, and M. Kamimura, Prog. Part. Nucl. Phys. **51** (2003), 223.

119) M. Yahiro, K. Ogata, and K. Minomo, Prog. Theor. Phys. **126** (2011), 167 [arXiv:1103.3976 [nucl-th]].

120) S. Hashimoto, M. Yahiro, K. Ogata, K. Minomo, and S. Chiba, Phys. Rev. C **83** (2011), 054617 [arXiv:1104.1567 [nucl-th]].

121) B. Abu-Ibrahim, W. Horiuchi, A. Kohama, and Y. Suzuki, Phys. Rev. C **77** (2008), 034607; W. Horiuchi, Y. Suzuki, B. Abu-Ibrahim, and A. Kohama, Phys. Rev. C **75** (2007), 044607.

122) W. Horiuchi, Y. Suzuki, P. Capel, and D. Baye, Phys. Rev. C **81** (2010), 024606.

123) A. M. Mukhamedzhanov and N. K. Timofeyuk, Yad. Fiz. **51** (1990), 679 [Sov. J. Nucl. Phys. **51** (1990), 431]; H. M. Xu, C. A. Gagliardi, R. E. Tribble, A. M. Mukhamedzhanov and N. K. Timofeyuk, Phys. Rev. Lett. **73** (1994), 2027.

124) T. Aumann *et al.*, Phys. Rev. C **59** (1999), 1252.

125) P. G. Hansen, Phys. Rev. Lett. **77**, 1016 (1996).

126) P. G. Hansen and J. A. Tostevin, Ann. Rev. Nucl. Part. Sci. **53**, 219 (2003).

127) Y. Kondo *et al.*, Phys. Rev. C **79** (2009), 014602.

128) E. K. Warburton and B. A. Brown, Phys. Rev. C **46** (1992), 923.

129) Y. Kondo *et al.*, Phys. Lett. B **690** (2010), 245.

130) M. Milin *et al.*, Nuclear Physics A **730** (2004), 285.

131) V. Lapoux *et al.*, Phys. Rev. C **66** (2002), 034608.

132) A. M. Kobos, B. A. Brown, P. E. Hodgson, G. R. Satchler, and A. Budzanowski, Nucl. Phys. A **384** (1982), 65.

133) E. F. Aguilera *et al.*, Phys. Rev. Lett. **84** (2000), 5058.

134) E. F. Aguilera *et al.*, Phys. Rev. C **63** (2001), 061603.

135) S. N. Ershov, B. V. Danilin, and J. S. Vaagen, Phys. Rev. C **62** (2000), 041001(R).

136) T. Kikuchi *et al.*, Phys. Lett. B **391** (1997), 261; T. Kikuchi *et al.*, Eur. Phys. J. A **3** (1998), 209.
137) N. Iwasa *et al.*, Phys. Rev. Lett. **83** (1999), 2910; F. Schümann *et al.*, Phys. Rev. Lett. **90** (2003), 232501.
138) J. N. Bahcall, M. H. Pinsonneault and Sarbani Basu, Astrophys. J. **555** (2001), 990 and references therein.
139) A. R. Junghans *et al.*, Phys. Rev. C **68** (2003), 065803.
140) T. Motobayashi, private communication (2004).
141) A. A. Junghans, K. A. Snover, E. C. Mohrmann, E. G. Adelberger, L. Buchmann, Phys. Rev. C **81** (2010), 012801(R).
142) E. D. Johnson *et al.*, Phys. Rev. Lett. **97** (2006), 192701.
143) T. Fukui, K. Ogata, and M. Yahiro, Prog. Theor. Phys. **125** (2011), 1193.
144) K. Ogata, M. Kan, and M. Kamimura, Prog. Theor. Phys. **122** (2009), 1055.
145) C. Angulo *et al.*, Nucl. Phys. A **656** (1999), 3.
146) K. Nomoto, Astrophys. J. **253** (1982), 798.
147) S. Ishikawa, J. Phys. Conf. Ser. **312** (2011), 042010.
148) A. Dotter and B. Paxton, Astronomy and Astrophysics 507 (2009), 1617.
149) T. Suda, R. Hirschi, and M. Y. Fujimoto, Astrophys. J. **741** (2011), 61.
150) M. Saruwatari and M. Hashimoto, Prog. Theor. Phys. **124** (2010), 925.
151) F. Peng and C. D. Ott, Astrophys. J. **725** (2010), 309.
152) Y. Matsuo, H. Tsujimoto, T. Noda, M. Saruwatari, M. Ono, M. Hashimoto, and M. Y. Fujimoto, Prog. Theor. Phys. **126** (2011), 1177.
153) P. Morel, J. Provost, B. Pichon, Y. Lebreton, and F. Thévenin, Astronomy and Astrophysics **520** (2010), A41.
154) Y. Kikuchi, M. Ono, Y. Matsuo, M. Hashimoto, and S. Fujimoto, Prog. Theor. Phys. **127** (2012), 171.
155) N. B. Nguyen, F. M. Nunes, I. J. Thompson, and E. F. Brown, arXiv:1112.2136 (nucl-th).
156) H. Matsui, in *Proceedings of the 23rd Symposium on Fusion Technology*, Venice, Italy, 20-24 Sept. (2004).
157) M. Hagiwara *et al.*, Fusion Sci. Technol. **48** (2005), 1320.
158) A. Y. Konobeyev, Y. A. Korovin, P. E. Pereslavtsev, U. Fischer, and U. von Möllendorff, Nucl. Sci. Eng. **139** (2001), 1.
159) U. Fischer, M. Avrigeanu, P. Pereslavtsev, S. P. Simakov, and I. Schmuck, J. Nucl. Mater. **367–370** (2007), 1531.
160) R. Serber, Phys. Rev. **72** (1947), 1008.
161) T. Ye, Y. Watanabe, and K. Ogata, Phys. Rev. C **80** (2009), 014604.
162) T. Ye, Y. Watanabe, K. Ogata, and S. Chiba, Phys. Rev. C **78** (2008), 024611.
163) J. Pampus *et al.*, Nucl. Phys. A **311** (1978), 141.
164) T. Ye, S. Hashimoto, Y. Watanabe, K. Ogata, and M. Yahiro, Phys. Rev. C **84** (2011), 054606.
165) Fusion Evaluated Nuclear Data Library FENDL 3.0, IAEA (http://www-nds.iaea.org/fendl3/).
166) S. Chiba, T. Fukahori, K. Shibata, B. Yu, and K. Kosako, Fusion Eng. Des. **37** (1997), 175.
167) T. Fukahori, S. Chiba, N. Kishida, M. Kawai, Y. Oyama, and A. Hasegawa, Status of JENDL Intermediate Energy Nuclear Data, Proceedings of the International Conference on Nuclear Data for Science and Technology, Trieste, Italy, 1997 (Societa Italiana di fisica), 899 (1997).
168) T. Matsumoto, D. Ichinkhorloo, Y. Hirabayashi, K. Katō, and S. Chiba, Phys. Rev. C **83** (2011), 064611.
169) S. Chiba *et al.*, Phys. Rev. C **58** (1998), 2205.
170) H. Hogue *et al.*, Nucl. Sci. Eng. **69** (1979), 22.
171) L. Hansen *et al.*, Phys. Rev. C **38** (1988), 525.
172) C. Louchart, A. Obertelli, A. Boudard, and F. Flavigny, Phys. Rev. C **83** (2011), 011601(R).
173) R. Crespo, A. Deltuva, and A. M. Moro, Phys. Rev. C **83** (2011), 044622.
174) Y. Suzuki and K. Ikeda, Phys. Rev. C **38** (1988), 410.
175) S. Aoyama, T. Myo, K. Katō, and K. Ikeda, Prog. Theor. Phys. **116** (2006), 1.